Investigating the Potential Role of Protocadherin-7 in Determining the Fate of Long-Term Hematopoietic Stem Cells

A Thesis

submitted to

Indian Institute of Science Education and Research Pune in partial fulfillment of the requirements for the BS-MS Dual Degree Program

by

AMISHA DEVAN

Indian Institute of Science Education and Research, Pune

Dr. Homi Bhabha Road,

Pashan, Pune 411008, India

Date: March, 2024

Under the guidance of

Supervisor: Dr. Linheng Li

Stowers Institute for Medical Research

Kansas City, Missouri, USA, 64110

From May 2023 to March 2024

Certificate

This is to certify that this dissertation entitled "Investigating the Potential Role of Protocadherin-7 in Determining the Fate of Long-Term Hematopoietic Stem Cells" towards the partial fulfillment of the BS-MS dual degree program at the Indian Institute of Science Education and Research, Pune represents study/work carried out by Amisha Devan at the Stowers Institute for Medical Research under the supervision of Dr. Linheng Li, during the academic year 2023-2024.

Dr. Linheng Li
Professor and Principal Investigator
Stowers Institute for Medical Research

Committee:

Project Supervisor: Dr. Linheng Li, Stowers Institute for Medical Research

TAC member: Dr. Girish Ratnaparkhi, Department of Biology, IISER Pune

This thesis is dedicated to my guiding force,

my Achan and Amma

Declaration

I hereby declare that the matter embodied in the report entitled “Investigating the Potential Role of Protocadherin-7 in Determining the Fate of Long-Term Hematopoietic Stem Cells” are the results of the work carried out by me at the Stowers Institute for Medical Research under the supervision of Dr. Linheng Li, and the same has not been submitted elsewhere for any other degree. Wherever others contribute, every effort is made to indicate this clearly, with due reference to the literature and acknowledgement of collaborative research and discussions.

Name of Student- Amisha Devan

Roll number- 20191006

Table of Contents

List of Figures

List of Tables

Abstract

Hematopoietic stem cells (HSCs) exhibit self-renewal and can differentiate into mature blood cells. Long-term HSCs (LT-HSCs) have long-term reconstitution potential to replenish the HSC pool. Based on reaction to stress, LT-HSCs have been categorized into quiescent reserve HSCs (rHSCs) located near N-Cadherin+ Mesenchymal Stem Cells in the endosteal niche and primed HSCs (pHSCs), which differentiate into short-term HSCs (ST-HSCs) and are located throughout the central marrow. Bulk-RNA sequencing of HSCs and their progeny revealed differential expression of Pcdh7, a non-clustered delta-1 protocadherin, with higher levels in pHSCs as compared to rHSCs. Pcdh7 can interact with other adhesion proteins to cause cell migration, which suggests a potential role in guiding LT-HSC migration away from the endosteal niche due to its increased expression. Flow cytometry analysis in transgenic mice with Pcdh7 tagged to ZsGreen indicates less expression of Pcdh7 protein in rHSCs and pHSCs, but notable expression in ST-HSCs. To confirm Pcdh7 expression within these HSCs, ZsGreen was observed within sorted cells which requires further validation. Immunofluorescence staining of femur sections identified a few ZsGreen+ cells within the bone marrow. This project aims to check if Pcdh7 plays a role in determining the fate that a LT-HSC attains.

Acknowledgements

As my master's thesis project comes to an end, I would like to take this opportunity to express my heartfelt gratitude to the individuals and institutions who have supported me on this journey.

To Dr. Linheng Li, who has been an extremely supportive and encouraging PI, offering invaluable words of wisdom, while consistently encouraging me to think outside the box.

To my mentor Ruochen and the members of the Linheng Li lab for their assistance in troubleshooting experiments and their constant guidance.

To Stowers Institute of Medical Research, for providing me with the best working environment any scientific researcher could ever dream of. The core facilities have some of the most brilliant scientists who are always up for challenges and never hesitate to assist with my experiments.

To Dr. Girish Ratnaparkhi, who encouraged me to pursue my project abroad and whose doors are always open for words of advice.

To IISER Pune, for providing me with the ideal venue for exploration and growth over the past five years.

To my roommates, Shruti and Ritvee, and friends from Kansas City- Lucy, Amruta, Sergio, and Mindy, who made my transition to a new city smooth and enjoyable.

To my dear friends Aryan, Sakshi, and Shyam, and my other close friends who have supported me and ensured my well-being, even from afar.

To my brother Amit, who always had my back, and my Kunjoonji, who always prayed for me.

And lastly, I am profoundly grateful to my parents Devan and Seeja, my guiding light, whose unwavering belief in me has shaped me into the person I am today.

Contributions

Contributor name	Contributor role
Dr. Linheng Li	Conceptualization, Ideas
Dr. Linheng Li, Ruochen Dong, Amisha Devan, Jeff Haug, Jose Javier Emmanuel, Amanda Kroesen, Zulin Yu, Seth Malloy, Shengping Huang, NatiCia Morris	Methodology
-	Software
Amisha Devan	Validation
Amisha Devan	Formal analysis
Amisha Devan	Investigation
Stowers Institute for Medical Research	Resources
-	Data Curation
Amisha Devan	Writing - original draft preparation
Dr. Linheng Li	Writing - review and editing
Amisha Devan	Visualization
Dr. Linheng Li, Ruochen Dong	Supervision
Dr. Linheng Li	Project administration
Dr. Linheng Li	Funding acquisition

CHAPTER 1- Introduction

1.1 Hematopoietic Stem Cells and Hematopoiesis

Hematopoietic stem cells (HSCs) stand at the forefront of blood cell production, functioning as multipotent stem cells that differentiate to give rise to mature blood cells of various lineages that are in circulation (Orkin and Zon, 2008). HSCs can self-renew and differentiate into lineage-restricted progenitors that progressively differentiate into different cell types including erythrocytes, lymphocytes, macrophages, and megakaryocytes (Laurenti and Göttgens, 2018) (Fig 1.1). Hematopoiesis, the process by which blood cells are replenished, is highly regulated as over-proliferation of HSCs can lead to diseases like leukemia while insufficient proliferation can lead to a depleted HSC pool.

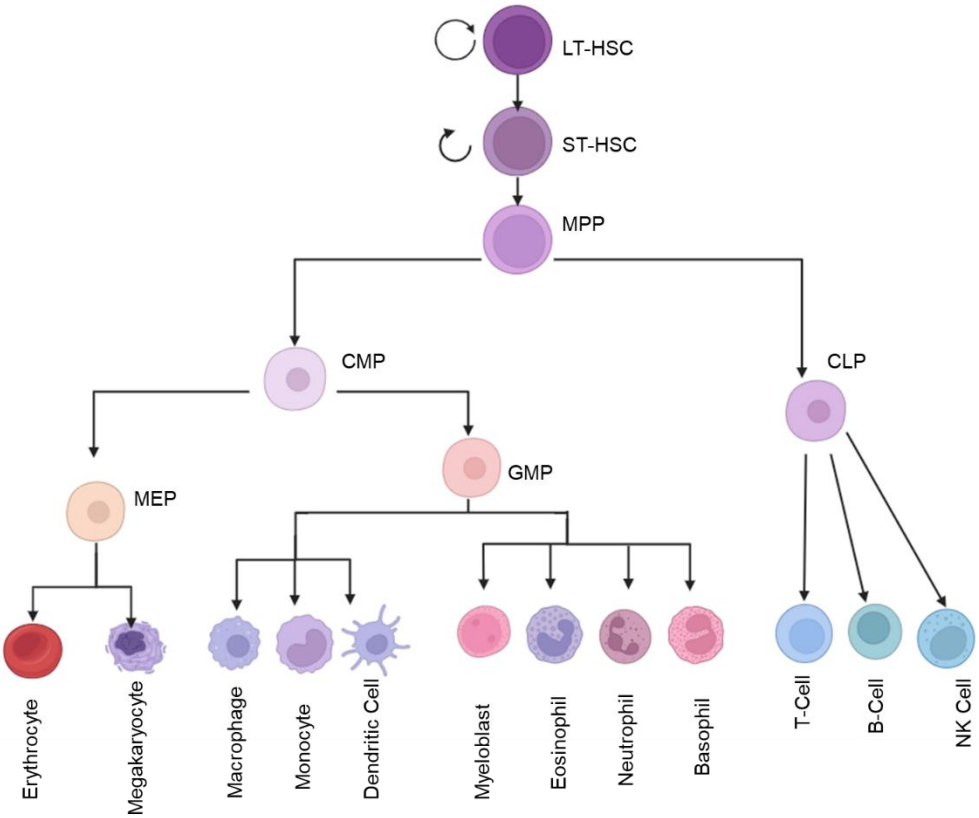

Figure 1.1: Hematopoiesis

Primitive hematopoiesis, which produces erythrocytes, megakaryocytes, and macrophage progenitors, occurs in the embryonic yolk sac by E7.5 to support the development of the growing embryo (Medvinsky *et al.*, 2011). Definitive hematopoiesis that gives rise to long-term repopulating cells first occurs in the developing embryo in the aorta-gonad mesonephros by E11 when the hemogenic endothelium undergoes an endothelial to hematopoietic transition to give rise to HSCs. The HSCs colonize the fetal liver which is the major hematopoietic organ during embryonic development. Hematopoiesis is finally established in the bone marrow by E16.5 which continues throughout adulthood (Gao *et al.*, 2018) (Fig 1.2)

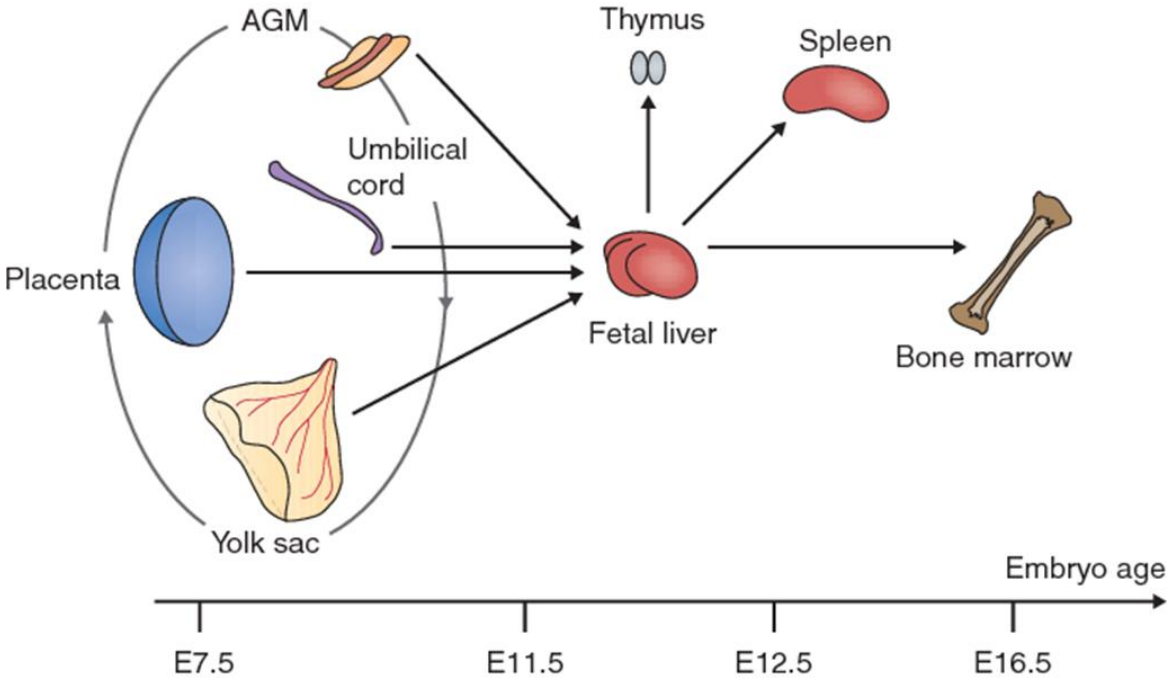

Figure 1.2: Fetal to adult murine hematopoiesis. Bone marrow is the primary location for hematopoiesis in the adult (Medvinsky, et.al. Development. 2011)

.

HSC behavior and fate have been studied over the years through transplantation of donor cells and colony formation assays (Till and McCulloch, 1961; Morrison *et al.*, 1995; Reya, 2003). Based on self-renewal ability and multipotential differentiation, they can be divided into two major subpopulations- Long-Term HSCs (LT-HSCs) and Short-Term HSCs (ST-HSCs). LT-HSCs have long-term reconstitution potential, are rare and quiescent, and can differentiate into ST-HSCs which are proliferative and have short-term reconstitution potential (Yang *et al.*, 2005; Yin and Li, 2006). Multipotent Progenitors (MPPs) arise from ST-HSCs which further differentiate into Common Lymphoid Progenitors (CLP) and Common Myeloid Progenitors (CMP) and are called hematopoietic progenitors (HPCs) in general (Kondo *et al.*, 1997; Morrison *et al.*, 1997; Akashi *et al.*, 2000; Yin and Li, 2006).

1.2 Hematopoietic stem cell niche and bone marrow architecture

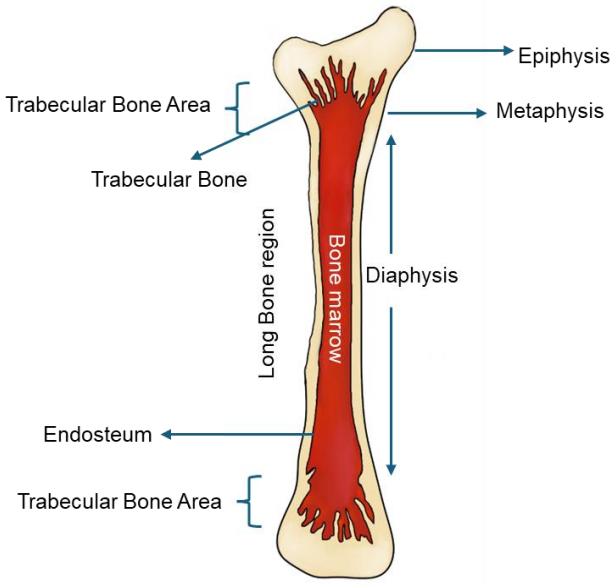

Figure 1.3: Structure of the mouse femur

Hematopoietic Stem Cell niches are the micro-environments that regulate the proliferation, cell fate, differentiation, and migration of HSCs. They help maintain the

balance between self-renewal and differentiation in the HSC pool (Li and Xie, 2005). The complexity of the stem cell niche and the heterogeneity within the HSC pool make it difficult to study the regulatory factors and the cellular components that control HSC activity in the niche (Pinho and Frenette, 2019). Studying the HSC niche and the mechanisms of maintenance of the HSC pool will facilitate the culture of HSCs ex-vivo which can be used as treatment for hematological malignancies.

Bone marrow (BM) is the primary location for hematopoiesis in adults and consists of cells that are of both hematopoietic and non-hematopoietic origin. The bone marrow is encapsulated within the cavities of the long bones and axial bones which have an inner lining called the endosteum. The endosteal cells include preosteoblasts, osteoblasts, osteoclasts, and osteocytes. (Yin and Li, 2006; Birbrair and Frenette, 2016). Within the femur, the trabecular bone area (TBA) of the metaphysis helps maintain the quiescence of hematopoietic stem cells and HPCs (Zhang *et al.*, 2003; Ellis *et al.*, 2011; Köhler *et al.*, 2009). The central marrow (CM) which lies throughout the diaphysis, is made of cortical bone and is the major region for the proliferation and differentiation of HSCs into mature blood cells (Yin and Li, 2006). The bone marrow is innervated by a network of sympathetic nerves and blood vessels including arterioles, sinusoids, and transition zone vessels. These form distinct zones in the bone marrow in association with other cells like perivascular reticular cells, Schwann cells, fibroblasts, and hematopoietic cells to spatially regulate HSCs (Lucas, 2021; Yang *et al.*, 2024).

1.3 Components and major players in the niche

The niche concept, proposed in 1978 by R. Schofield, suggests that the environment where stem cells are located determines their fate (Schofield, 1978). The components of the HSC niche include both HSCs, their progeny, and non-hematopoietic cells. The endosteal cells are the first component of the HSC niche to be identified. Initial studies suggested that spindle-shaped N-Cadherin positive cells that line the osteoblasts, which are different from the oval shaped osteoblasts, an important regulatory component of HSC niche, as increase in their number led to an increase in number of HSCs observed (Calvi

et al., 2003; Zhang *et al.*, 2003). When HSCs were purified and transplanted into mice that were irradiated, they tended to home near the N-Cadherin+ niche cells in the endosteal region. In contrast, the distribution of transplanted HSCs was random within the bone marrow in non-irradiated mice (Xie *et al.*, 2009).

Blood vessels like arterioles and sinusoids were also found to be crucial components of the HSC niche called the vascular niche as they secrete factors that help in HSC hematopoiesis and help mature blood cells to move into circulation (Yin and Li, 2006). 60% of HSCs characterized by the expression of SLAM markers like CD150, CD48 and CD41, were seen to be mostly localized near the sinusoidal epithelium, while 16% were also found near the endosteum (Kiel *et al.*, 2005).

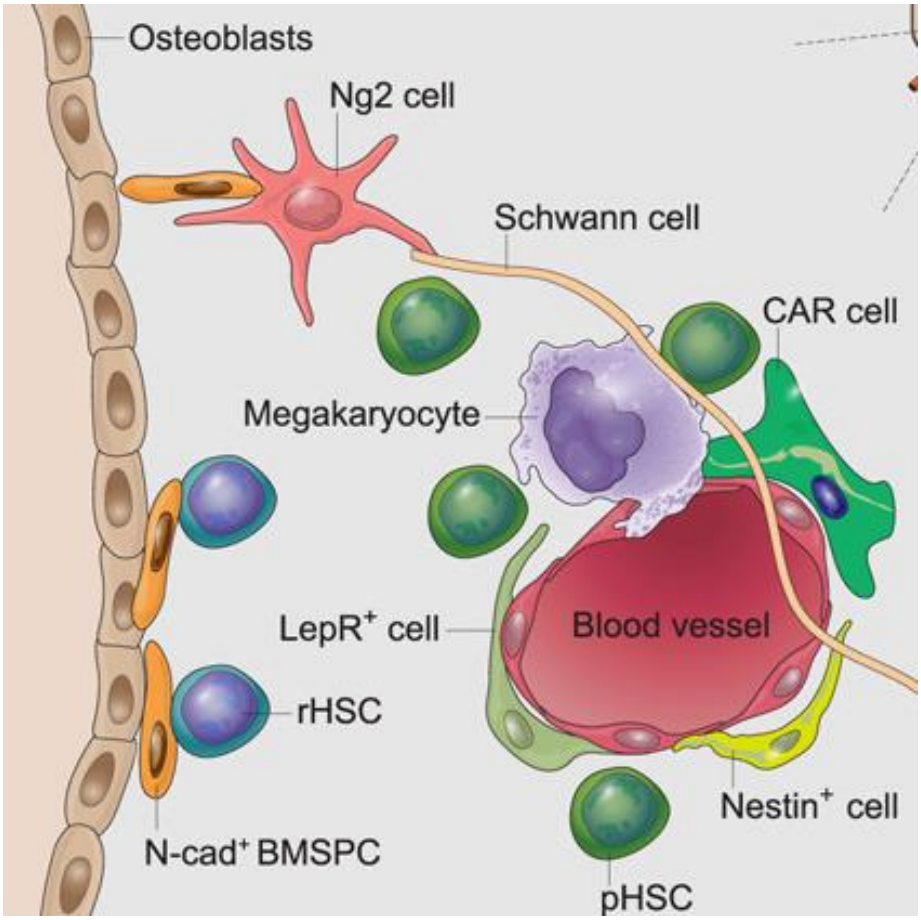

Figure 1.4: Some of the major players in the HSC niche include HSCs, endosteal cells, Mesenchymal stem cells (BMSPCs), arterioles, sinusoids, megakaryocytes, Schwann cells and CXCL12 Abundant Reticular (CAR) cells (Zhao et al. *Cell Reports*. 2019)

Chemokines play an important role in regulation of HSC proliferation and maintenance and are secreted by various cellular components of the HSC niche. CXC chemokine ligand 12 or CXCL12, by binding to its receptor CXCR4 on HSC surface, causes homing of HSCs and supports their maintenance. SCF or Kit ligand binds to the Kit receptor on HSCs on HSCs to support HSC proliferation and survival (Ding *et al.*, 2012).

Mesenchymal Stem Cells (MSCs) are stromal cells with a potential to give rise to osteoblasts, adipocytes, and chondrocytes (Zhao *et al.*, 2019). MSCs were discovered to support hematopoiesis in the bone marrow. HSCs were found homing to either N-cadherin+ MSCs at the TBA (Xie *et al.*, 2009) or to Nestin+ MSCs that have a perivascular distribution throughout the bone marrow (Méndez-Ferrer *et al.*, 2010). These MSCs express core HSC maintenance genes and factors like CXCL-12, Kit ligand, and Angiopoietin-1 (Méndez-Ferrer *et al.*, 2010). N-Cad+ MSCs can provide a protective harbor for quiescence of LT-HSCs (Zhao *et al.*, 2019; Yang *et al.*, 2024). CXCL12-abundant reticular cells (CAR) cells surrounding the sinusoidal endothelial cells were seen to secrete high levels of CXCL-12 and Kit ligand. HSCs were found in large numbers near the CAR cells at the perivascular niche (Sugiyama *et al.*, 2006) and were seen to be largely (~80%) lost when SCF was deleted from endothelial cells and perivascular cells in the bone marrow (Ding *et al.*, 2012).

HSCs are also found in close contact with Non-myelinating Schwann cells in the bone marrow, as they secrete an activated form of TGF-β that keeps HSCs quiescent. (Yamazaki *et al.*, 2011). However, the main source of TGF-β in BM are megakaryocytes of hematopoietic origin. Megakaryocytes play a role in maintaining HSCs in a temporary quiescent state through secretion of TGFβ and CXCL4 (Zhao *et al.*, 2014; Bruns *et al.*, 2014)

1.4 Reserve and Primed Long-Term HSCs

LT-HSCs can be functionally categorized based on their response to stress such as myeloablation: as primed HSCs (pHSCs) that are sensitive to myeloablation and reserve HSCs (rHSCs) that remain unaffected and play a role in restoring the depleted HSC pool.

rHSCs express higher levels of genes responsible for quiescence such as p57, while pHSCs express relatively higher levels of cell proliferation-related genes including Myc. pHSCs are located throughout the central marrow and serve as a transition state between rHSCs and cycling ST-HSCs. rHSCs are predominantly localized near N-Cad+ MSCs in the TBA, which helps to preserve the rHSC pool during stress. However, the adhesion proteins that link rHSCs to the N-cad+ MSCs at the endosteal niche remain largely unknown (Zhao et al., 2019).

1.5 Protocadherins

Cadherins are a family of transmembrane glycoproteins that are Ca^{2+} dependent and modulate cell-cell adhesion and morphogenesis (Takeichi, 1988; Hirano and Takeichi, 2012). The cadherin superfamily encompasses various subfamilies, such as type I and type II Classical Cadherins, desmosomal cadherins, protocadherins, flamingo/CELSR, and cadherin-related proteins (Hulpiau and van Roy, 2009). These subfamilies are characterized by multiple cadherin motifs within their extracellular domain.

Protocadherins are the largest subfamily of Cadherins. The discovery of Pcdhs goes back to 1993, when new cadherin-like sequences were found, with six or seven cadherin repeats instead of five in their ectodomain, as well as a transmembrane domain and a unique cytoplasmic tail which was not the same in all Pcdhs (Sano *et al.*, 1993). The name “protocadherins” was given to these proteins which are phylogenetically different from classical cadherins but resemble primordial cadherins (Sano *et al.*, 1993; Hulpiau and van Roy, 2009). Defects in protocadherins are seen to cause neurological disorders, impaired development, and tumorigenesis (Hirabayashi and Yagi, 2014; Pancho *et al.*, 2020). Protocadherins are divided into clustered and non-clustered protocadherins based on the clustering of the genes within chromosomes. Clustered protocadherins have their exons tandemly clustered on the same chromosome (Wu and Maniatis, 1999), and diverse isoforms of protocadherins can be translated depending on the promoter chosen and alternative splicing (Yagi, 2012). Non-clustered protocadherins are scattered throughout

the genome and are classified as δ-0, δ-1 and δ-2 protocadherins based on conservation of amino-acid motifs, homology and the number of cadherin domains (Redies *et al.*, 2005; Vanhalst *et al.*, 2005; Hulpiau and van Roy, 2009). The extracellular domains of protocadherins can mediate homophilic trans interactions with themselves and heterophilic interactions with other members of the cadherin superfamily to control adhesion and growth. Some Pcdhs can also form heterophilic cis interactions.

1.6 Protocadherin-7

Pcdh7 or Protocadherin-7 is a transmembrane δ-1 protocadherin whose extracellular domain contains seven cadherin domain repeats, one of which contains the binding site for cell-cell adhesion. It is predicted that these interactions may dictate cell adhesion, motility, and cell-cell interaction and support downstream signalling. As Pcdh-7 is highly expressed in the brain and heart cells, it is given the name Brain-Heart protocadherin (BH-Pcdh) (Yoshida *et al.*, 1998). In Xenopus, NF-protocadherin, which is a homolog of Pcdh7, plays a role in neural tube enclosure by the ectoderm and axon elongation in the ganglion cells of the retina (Piper *et al.*, 2008; Rashid *et al.*, 2018). The role of Pcdh-7 in cell adhesion or repulsion is suggested to be very cellular context-specific, depending on the interacting protein and the ratio of expression of the two adhesion proteins (Bisogni *et al.*, 2018). In patients with gastric cancer, Pcdh-7 is down-regulated to promote cell migration as it inhibits E-Cadherin (Chen *et al.*, 2017). In neurons, Pcdh7 regulates dendritic spine morphology, and its overexpression results in the collapse of dendrites (Wang *et al.*, 2020b). Pcdh-7 can inhibit cell-cell adhesion to prevent the formation of homotypic cell-in-cell structures in tumors (Wang *et al.*, 2020a).

From bulk-RNA sequencing in HSCs and their progeny cells, we observe that there is a 1.5-fold increase in the expression of Pcdh7 in pHSCs as compared to rHSCs (Fig 1.5). ST-HSCs show higher expression of Pcdh7 relative to rHSCs, though the levels remain lower than those observed in pHSCs. Other members of the cadherin superfamily do not exhibit significant differences in expression between rHSCs and pHSCs. Figure 1.6 shows

the RNA expression for 8 Cadherin superfamily genes that have the highest differential expression between rHSCs and pHSCs.

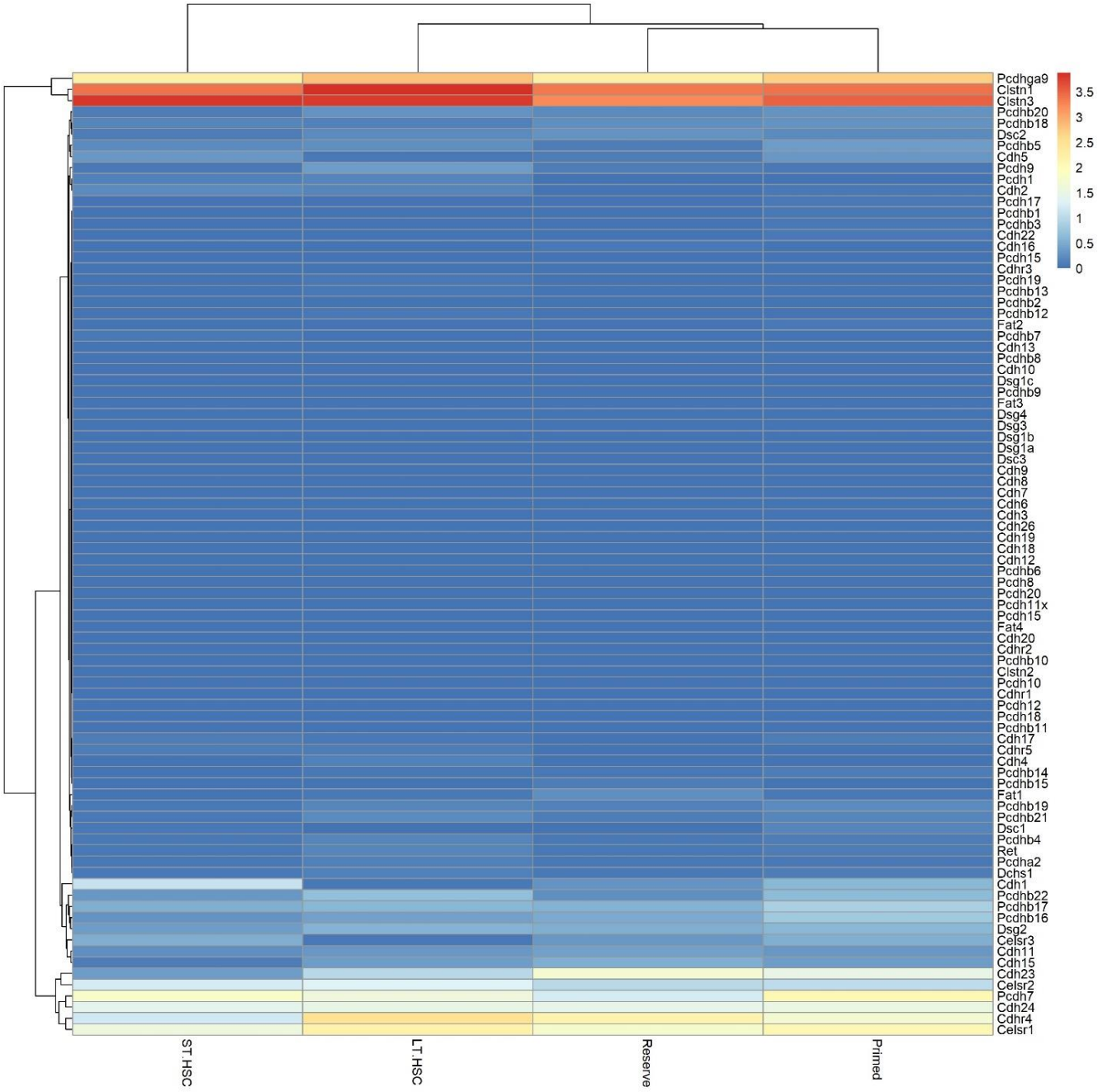

Figure 1.5: Bulk-RNA sequencing data of Cadherin superfamily proteins for rHSCs, pHSCs, LT-HSCs and ST-HSCs

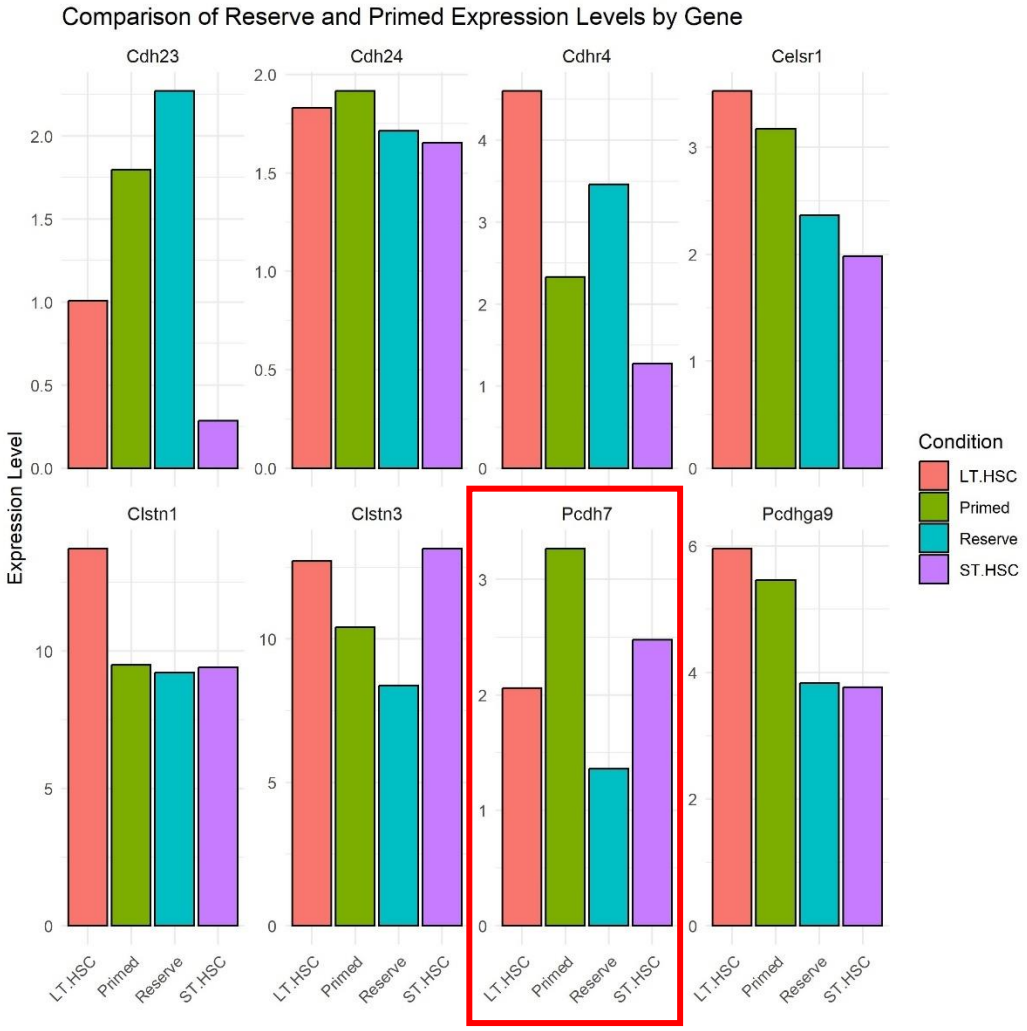

Figure 1.6: RNA expression levels for 8 of the most differentially expressed Cadherin family genes between rHSCs and pHSCs. Pcdh7 is expressed 1.5-fold higher in pHSCs as compared to rHSCs.

1.7 Aim of the project

This study aims to investigate if Pcdh7 can have a role in determining the fate of LT-HSCs and if Pcdh-7 expressing HSCs are pHSCs that associate with the vascular niche. rHSCs divide asymmetrically to produce daughter cells. We hypothesize that one of these cells will express higher levels of Pcdh7 protein. A rise in Pcdh7 expression may alter the adherence of the daughter cell to N-Cad+ MSCs through interactions with other adhesion

proteins, which could facilitate its migration from the endosteal niche into the central marrow and potentially lead the cell to take on the fate of a pHSC. The cell, under the right conditions, can eventually differentiate into an ST-HSC. Subsequently, the daughter cell residing in the endosteal niche may develop the fate of an rHSC with additional niche components contributing to this outcome.

A transgenic reporter mouse line (Pcdh7-ZsG) has been engineered for this study, in which the Pcdh7 protein will be translated along with a ZsGreen fluorescent protein tag. The expression of the Pcdh7 protein on HSCs will be validated using flow cytometry analysis and the subsets of HSCs that are Pcdh7-ZsGreen+ will be identified and quantified. For further validation, different subpopulations of HSCs will be sorted, fixed, and stained using an anti-ZsGreen antibody and will be imaged to check ZsGreen expression. To better understand the localization of Pcdh7-ZsGreen+ HSCs within the bone marrow, whole-mount immunostaining of mouse femur and immunofluorescence staining of tissue sections will be performed. Ex-vivo Imaging Stem cells (EVISC) (established by Xie *et al.*, 2009) which enables the study of bone marrow cells outside the hose in real-time will be used to study the behavior, migration, and proliferation of Pcdh7-ZsGreen+ HSCs within the bone marrow. Through studying the expression of Pcdh7, we hope to understand the role of adhesion proteins in the hematopoietic process.

.

CHAPTER 2- Materials and Methods

2.1 Genetic engineering of transgenic mice

A transgenic strain of mouse has been genetically engineered by using CRISPR/Cas-9 to knock-in the gene coding for ZsGreen fluorescent protein before the stop codon of the *PCDH7* gene on chromosome 5 in C57BL/6 mice (courtesy Genomic engineering, Transgenic and Reproductive technologies, SIMR). The resulting Pcdh7-ZsGreen strain (Pcdh7-ZsG) has ZsGreen tagged to 3' end of exon 3 of the *PCDH7* gene using a 4 amino acid spacer, and on translation, ZsGreen is attached to the C-terminal of the transmembrane Pcdh7 protein, making it intracellular.

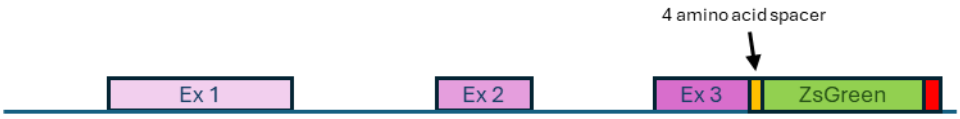

Figure 2.1 Genetic engineering of Pcdh7-ZsG reporter mouse. Gene coding for ZsGreen is attached to the 3' end of *PCDH7* gene using a 4-amino acid spacer.

2.2 Flow Cytometry Analysis

Flow cytometry analysis is used to check the presence of Pcdh7-expressing subpopulations within HSCs and to quantify the number of the Pcdh7+ HSCs.

2.2.1 Preparation of single cell suspension of bone marrow

Mice of the required age group are euthanized, and femurs and tibias are collected. Bone marrow is flushed out from the bones (till they turn pale) using a 20 1/2G syringe into 1X PBS + 1% FBS to create a single-cell suspension. The suspension is passed through a 40um nylon filter and centrifuged at 500g for 5 minutes at 4°Celsius, and the supernatant is discarded.

To lyse red blood cells, prewarmed RBC lysis solution is added to the cell pellet (Table 2.1). 2ml RBC lysis solution is added per sample and is incubated for 5 minutes at 37°

Celsius. The mixture is diluted with 1X PBS+ 1% FBS to ten times the volume of RBC lysis solution added and centrifuged at 500g for 5 minutes at 4° Celsius. The pellet is suspended in 1X PBS+ 1% FBS and filtered using a 20um syringe filter. The concentration of the cell suspension is adjusted to $1x10^7$ cells/ml after counting using a fluorescence cell viability counter (Cellometer® K2)

Table 2.1 Recipe for RBC lysis solution

Component	**Volume/mass**
Ammonium chloride	8.3 g
Sodium Bicarbonate	1.0 g
0.5M EDTA	200 µl
Deionized water	1 litre

2.2.2 Staining cell suspension for flow cytometry

For cytometry analysis on the Cytek® Aurora (Cytek Biosciences), controls for color compensation and fluorescent minus one (FMO) are prepared for each fluorophore alongside the sample. Color compensation controls, which are used to compensate the spectral overlap between different fluorophores, are prepared on antibody capture beads for each fluorophore, except DAPI which is compensated using wildtype cells instead of beads for staining. The staining panel (Table 2.2) includes an antibody dilution of 0.25-5 ug antibody per million cells. Suitable primary antibodies conjugated to fluorophores are selected to reduce the spectral overlap between fluorophores. DAPI is added at a concentration of 5ng per ml. To stain cells expressing lineage markers (CD3, CD4, CD8, B220, CD11b, Ter119, Gr-1, IgM), a lineage cocktail is prepared. The samples and controls are incubated along with the antibodies for 45 minutes on ice, washed using 1X PBS, and centrifuged at 500g for 5 minutes. The supernatant is discarded, and the pellet

is resuspended in 1X PBS. The samples and the controls are resuspended in the required volume of PBS and analyzed using the Cytek Aurora spectral flow cytometer. The data collected is analyzed using FCS Express™ Research Edition (De Novo Software) to identify the Pcdh7+ HSCs and quantify their numbers.

Table 2.2 Antibody panel used for flow cytometry.

Marker	Fluorophore for Zsgreen reporter mice	Fluorophore for WT mice
Lineage cocktail	PE-Cy5	PE-Cy5
Sca1	PE-Cy7	PE-Cy7
cKit	AF700	APC
Flk2	APC	PE
CD34	eFluor 450	eFluor 450
CD48	APC-Cy7	APC-Cy7
CD49b	PE	FITC
Pcdh7	endogenous ZsGreen	Alexa Fluor 700

Table 2.3 Reagents for flow cytometry

Name	Host species	Concentration	Source	Catalog number
CD3e Monoclonal Antibody (145-2C11), PE-Cyanine5	Armenian Hamster	0.2 mg/mL	eBioscience	Catalog # 15-0031-83
CD4 Monoclonal Antibody (RM4-5), PE-Cyanine5	Rat	0.2 mg/mL	eBioscience	Catalog # 15-0042-83

CD8a Monoclonal Antibody (53-6.7), PE-Cyanine5	Rat	0.2 mg/mL	eBioscience	Catalog # 15-0081-83
Ly-6G/Ly-6C (Gr-1) Monoclonal Antibody (RB6-8C5), PE-Cyanine5	Rat	0.2 mg/mL	eBioscience	Catalog # 15-5931-83
CD45R (B220) Monoclonal Antibody (RA3-6B2), PE-Cyanine5	Rat	0.2 mg/mL	eBioscience	Catalog # 15-0452-83
CD11b Monoclonal Antibody (M1/70), PE-Cyanine5	Rat	0.2 mg/mL	eBioscience	Catalog # 15-0112-83
TER-119 Monoclonal Antibody (TER-119), PE-Cyanine5	Rat	0.2 mg/mL	eBioscience	Catalog # 15-5921-83
IgM Monoclonal Antibody (II/41), PE-Cyanine5	Rat	0.2 mg/mL	eBioscience	Catalog # 15-5790-82
Ly-6A/E (Sca-1) Monoclonal Antibody (D7), PE-Cyanine7	Rat	0.2 mg/mL	eBioscience	Catalog # 15-5981-82
Alexa Fluor® 700 anti-mouse CD117 (c-Kit) Antibody	Rat	0.5 mg/mL	BioLegend	Catalog # 105846
CD135 (Flt3) Monoclonal Antibody (A2F10), PE	Rat	0.2 mg/mL	eBioscience	Catalog # 135310
APC anti-mouse CD135 Antibody	Rat	0.2 mg/mL	BioLegend	Catalog # 12-1351-82

CD34 Monoclonal Antibody (RAM34), eFluor™ 450	Rat	0.2 mg/mL	eBioscience	Catalog # 48-0341-82
APC/Cyanine7 anti-mouse CD48 Antibody	Armenian Hamster	0.2 mg/mL	BioLegend	Catalog # 103432
PE anti-mouse CD49b Antibody	Armenian Hamster	0.2 mg/mL	BioLegend	Catalog # 103506
CD49b (Integrin alpha 2) Monoclonal Antibody (DX5), FITC	Rat	0.2 mg/mL	eBioscience	Catalog # 11-5971-82
PCDH7 Antibody (OTI1F7) [Alexa Fluor® 700]	Mouse	0.2 mg/mL	Novus Biologicals	Catalog # 73269AF700
DAPI, dilactate		5 mg/ml	ThermoFisher Scientific	D3571
VersaComp Antibody Capture Kit, 2 Vials, LUO	N/A	N/A	Beckman Coulter	B22804

2.3 Flow cytometry sorting of HSCs

To sort different subsets of HSCs, the size of the sample to be sorted is prepared according to the target number of cells to be studied. Colour compensation controls are prepared on wildtype cells instead of beads. The concentration of DAPI added is adjusted to 5 µg/ml. The cells are sorted on the BD FACSymphony™ S6 Cell Sorter (BD Biosciences)

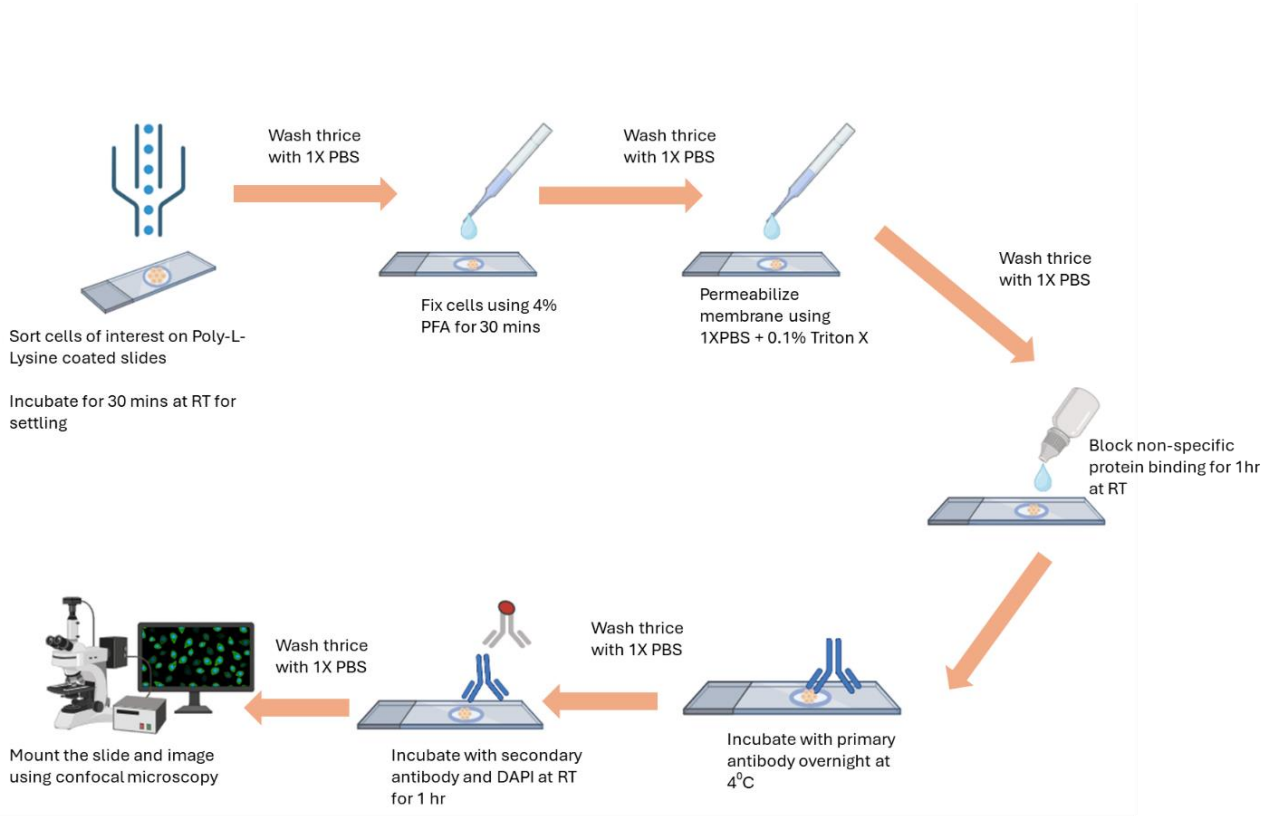

Figure 2.2 Protocol for immunofluorescence staining of single cells after flow cytometry sorting.

2.4 Immunofluorescence staining of single cells after flow cytometry sorting

Following FACS sorting of the population of interest, sorted cells are collected into 1.5 ml Eppendorf tubes in 100 µl of 1X PBS +1 % FBS and centrifuged at 500g for 10 5 minutes at 4°Celsius to form cell pellets. Most of the supernatant is carefully removed, leaving approximately 50-100 µl of PBS with the cells. The cells are resuspended in PBS and transferred to poly-L-lysine-coated slides within a small area marked by a PAP pen border. The cells can settle down by incubating the slides at room temperature in a moisture chamber for 30 minutes. Following this, PBS is slowly removed, and 4% PFA is added to fix cells for 15 minutes at room temperature. The fixed cells are then washed twice with 1X PBS and permeabilized using 1X PBS + 0.1% Triton X, incubating for 15 minutes. After removal of the liquid, cells are washed three times with 1x PBS and subsequently treated with a universal protein block at room temperature for 30 minutes. Following three washes with 1X PBST, cells are incubated with primary antibody at a dilution of 1:100 in antibody diluent for 1 hour at room temperature. After three additional

washes with 1x PBS, secondary antibody is added at a dilution of 1:1000 in antibody diluent and incubated for 1 hour at room temperature. Cells are then washed thrice with 1X PBS and stained with DAPI for 1 min, followed by a single wash with 1x PBS. ProLong Gold Antifade Mountant is applied to cover the sample, a cover slip is placed on top, and the slides are incubated at room temperature in the dark overnight. The samples are imaged using ZEISS LSM 980 with Airyscan 2 and Nikon CSU W1 confocal microscopes. Imahge analysis is done using ImageJ software.

2.5 Immunofluorescence staining of tissue sections

Immunofluorescence staining allows to study the localization of different cells within the bone marrow by staining them against different markers.

2.5.1 Preparation of tissue sections for immunofluorescence staining

Mouse femurs are collected from 6-8-week-old mice. The femurs are rinsed with 1X PBS, fixed in 4 % (v/v) paraformaldehyde (4% PFA) for 7-8 hours at 4° Celsius. decalcified using formic acid and dehydrated overnight in a solution of 30% sucrose in PBS. The bones are embedded in OCT, are cryo frozen, and 10 µm sections are obtained via parasagittal cuts using a cryotome. These sections can be stored at -80°C for future use.

To obtain brain sections, the mice are anesthetized and perfused using 4% PFA. The brain is harvested and dehydrated in 30% sucrose in PBS. After embedding in OCT (Tissue-Tek), it is cryo frozen and 10um sagittal sections are obtained using a cryostat (Leica).

2.5.2 Immunofluorescence Staining

The tissue sections are thawed and rehydrated through 5-minute 1X PBST washing. A hydrophobic barrier is applied around each section using a PAP pen. Non-specific binding of antibodies is prevented by incubating with a commercially available universal blocking reagent for one hour at room temperature. After 5-minute washes with 1X PBST, freshly prepared primary antibody dilutions (1:100 in antibody diluent) are added to the sections

and incubated overnight at 4° Celsius. Following washes, secondary antibody dilutions (1:1000 in antibody diluent) are added to the sections and incubated for one hour. After washes with 1X PBST and a final wash with 1X PBS, DAPI (1:500 dilution in PBS) is added to the section. The tissue sections are mounted using a cover slip with a mounting medium and then imaged using a confocal microscope. Image analysis is done using ImageJ software.

2.6 Whole mount Immunofluorescence staining

Femurs are harvested from mice aged 8-12 weeks and fixed in 4% (v/v) PFA for 7-8 hours at 4 degrees Celsius with gentle shaking. The fixed femurs are washed with 1x PBS and cryoprotected by incubating in a 30% (w/v) sucrose in PBS solution overnight at 4°C with continuous shaking. The cryoprotected bones are embedded in OCT and longitudinally bisected using a cryostat (Leica). The bone is trimmed till the bone marrow is visible and the bone becomes almost bisected. To remove the OCT, the bone is washed using 1X PBS.

Whole-mount immunostaining is performed in Eppendorf tubes on a rotator at room temperature. A stock of staining solution with 10% (v/v) dimethyl sulfoxide, 0.5% (v/v) IgePal630 (Sigma), and 5% (v/v) donkey serum (Jackson Immuno) in 1x PBS is prepared. The bones are blocked overnight in 1ml of staining solution containing 1% (v/v) BlokhenII (Aves Labs) at room temperature. After blocking the non-specific antibodies, primary antibodies are added at a concentration of 1:100 in staining solution and the bones are incubated for 3 days at room temperature with the primary antibody staining solution. The bone is washed at least 4-5 times at 30-minute intervals in 1x PBS at room temperature. The bones are incubated with secondary antibodies at a concentration of 1:100 in staining solution for 3 days at room temperature.

For tissue clearing, the bones are subjected to a series of graded ethanol concentrations for dehydration. The bones are incubated in 50%, 70%, 80%, and 95% (v/v) Ethanol dilutions for 10 minutes each, followed by overnight incubation in 100% ethanol. 100% ethanol is replaced with freshly prepared BABB (1:2 Benzyl Alcohol: Benzyl Benzoate),

and the solution is changed every 20-30 minutes until the bone becomes clear. Finally, the whole-mount bone is placed on a Mat-Tek dish containing BABB with the marrow side facing the coverslip for imaging using the LSM 980 confocal microscope.

Table 2.4 Reagents for immunofluorescence staining

Antibody	Host	Source	Catalog Number
Living Colors® Full-Length ZsGreen Polyclonal Antibody	Rabbit	TaKaRa	632474
N-Cadherin Antibody (13A9)	Mouse	Novus Biologicals	NBP1-48309SS
DAPI	N/A	Sigma Aldrich	D9542
Donkey anti-Rabbit IgG (H+L) Highly Cross-Adsorbed Secondary Antibody, Alexa Fluor™ 546	Donkey	ThermoFisher Scientific	A10040
Donkey anti-Mouse IgG (H+L) Highly Cross-Adsorbed Secondary Antibody, Alexa Fluor™ 546	Donkey	ThermoFisher Scientific	A10036
Donkey anti-Rabbit IgG (H+L) Highly Cross-Adsorbed Secondary Antibody, Alexa Fluor™ 647	Donkey	ThermoFisher Scientific	A31573
Antibody diluent Reagent	N/A	Life Technologies	3218
N-Cadherin Antibody (13A9)	N/A	BioGeneX	HK085-GP

2.7 Ex- Vivo Imaging Stem Cell (EVISC)

Ex- vivo imaging stem cells (as established by Xie et al., 2009) will be used to study HSC behavior in the bone marrow outside the host.

2.7.1 Preparation of sample

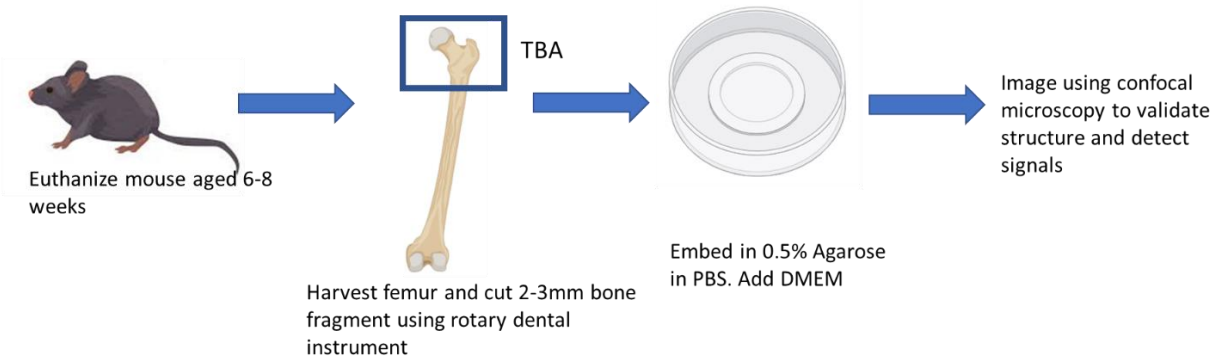

Figure 2.3: Protocol for EVISC imaging

Mice aged 6-8 weeks are euthanized and femurs are harvested. Using a rotary dental instrument (NTI-Kahla), bone fragments of 2-3 mm height are cut in a plane vertical to the bone. The bone fragments are embedded in 0.5% (w/v) Agarose in PBS with the open end of the bone facing the coverslip bottom of a MatTek dish. DMEM medium (without Phenol red, A1443001) is added to the bone culture. The bone fragments are imaged under LSM 980 confocal microscope to check if the bone architecture is intact and if fluorescently tagged cells can be visualized under the setup.

2.7.2 Setup of Spectral Imaging in LSM 980

The spectral imaging configuration of LSM 980 is used to identify the emission wavelength of the signal detected in the sample. Linear unmixing post-acquisition is used to segregate mixed fluorescence signals from dyes and cellular autofluorescence. Two-photon excitation is further used to separate fluorophores from autofluorescence. The secondary harmonic signal from collagen can be used to identify bone.

CHAPTER 3- Results

3.1 Confirmation of ZsGreen fluorescent protein expression by imaging of hippocampal sections.

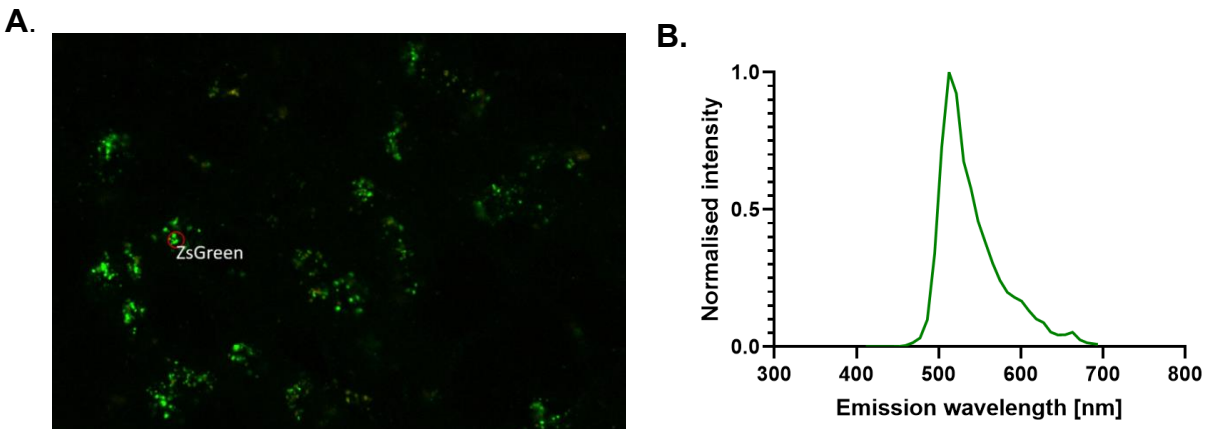

Figure 3.1: Spectral imaging of Hippocampal sections A) Hippocampal sections from Pcdh7-ZsG mice imaged at 40X magnification. Green signals seen are ZsGreen tagged to Pcdh7 in the neurons. B) Spectral unmixing of the green signal gives

According to published literature, Pcdh7 protein is highly expressed in the neurons and astrocytes of the brain and is shown to regulate dendritic spine morphology. To confirm the expression of ZsGreen fluorescent protein in Pcdh7-ZsG reporter mice, cryo sections of the hippocampus were obtained and were imaged using confocal microscopy. Upon excitation by the 488nm laser, distinct green patches like neuronal Pcdh7 expression were visible (Fig 3.1.A). Spectral unmixing of this green signal revealed an emission spectrum that peaked at 506nm, consistent with the expected emission peak for ZsGreen (Fig 3.1.B)

On immunofluorescence staining of the hippocampal sections with a commercially available anti-ZsGreen primary antibody, there is an 80% overlap between the anti-ZsGreen antibody signal and endogenous ZsGreen signal, suggesting a specificity for the antibody against ZsGreen which allows its usage for further immunofluorescence staining

experiments to amplify the ZsGreen signal. ZsGreen is observed around the DAPI staining in the cells, which is consistent with the transmembrane localization of Pcdh7 protein (Fig 3.2)

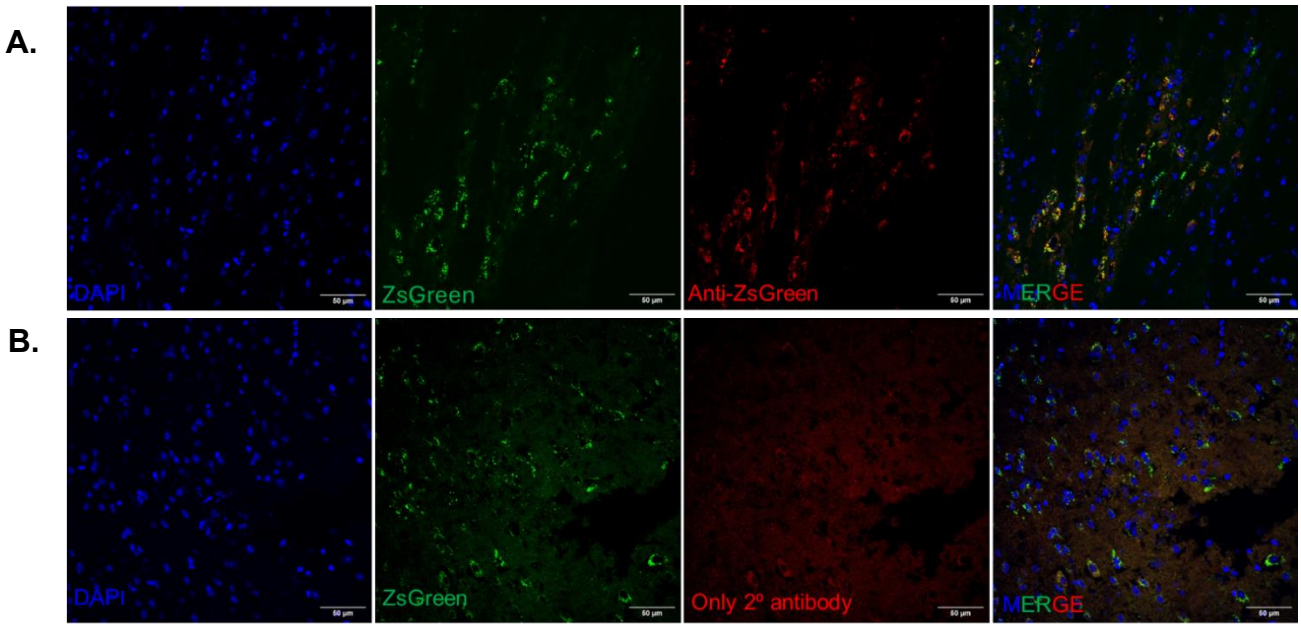

Figure 3.2: Immunofluorescence staining of hippocampal tissue sections. Blue represents DAPI and green represents the endogenous ZsGreen. A) anti-ZsGreen primary antibody was tagged was targeted by Alexa Fluor 647 secondary antibody. Anti-Zsgreen signal overlaps with endogenous ZsGreen. B) only secondary antibody was used.

3.2. Flow Cytometry analysis of Pcdh7+ HSCs suggests few HSCs express Pcdh7

Bulk-RNA sequencing studies from the lab suggest that pHSCs have higher RNA expression levels of Pcdh7 as compared to rHSCs. To validate the expression of the Pcdh7 protein and to identify the subtypes of HSCs that express the protein, flow cytometry analysis was utilized. Two distinct approaches were taken to characterize the Pcdh7+ HScs; i) to analyze the HSCs that express Zsgreen in Pcdh7-ZsG strain, as Zsgreen is tagged to Pcdh7, which gives an indirect quantification of the Pcdh7 HSCs and ii) the use of an anti-Pcdh7 antibody to identify Pcdh7+ HSCs in C57BL/6 (WT) mice. Six different cell populations were analyzed: Lin- cells, LSKs, LT-HSCs, ST-HSCs,

rHSCs, and pHSCs. The cellular markers used to identify the different subtypes are given in Fig 3.3. HSCs were characterized as Flk2- Lin- Sca1+ cKit+ (LSK) cells, with long-term HSCs (LT-HSCs) identified as LSK Flk2- CD34- CD48- cells, and short-term HSCs (ST-HSCs) as LSK Flk2- CD34+ CD48-. rHSCs were classified as LSK Flk2- CD34- CD48- CD49b- and pHSCs as LSK Flk2- CD34- CD48- CD49b+.

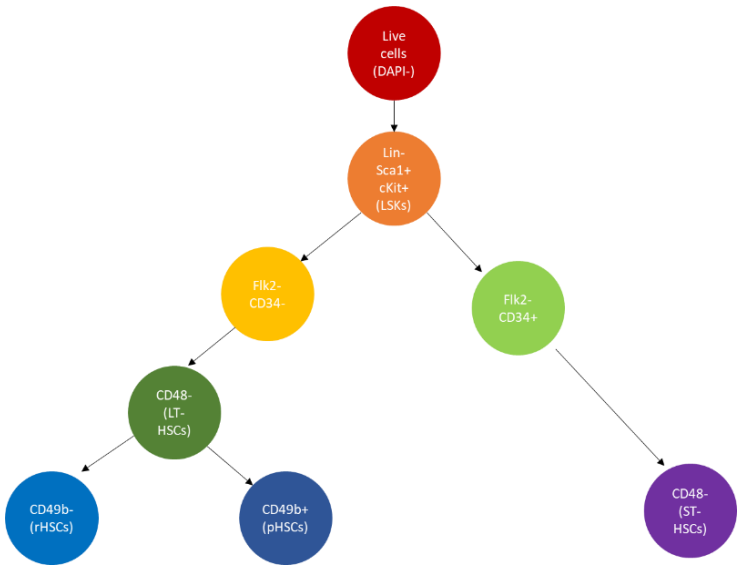

Figure 3.3: Cellular markers to Identify different HSC subpopulations.

3.2.1 Flow cytometry analysis of Pcdh7-ZsG strain

The bone marrow from homozygous Pcdh7-ZsG reporter mice was analyzed for Zsgreen+ HSCs to quantify cells that express Pcdh7. Two independent flow cytometry experiments were conducted. Experiment 1 used a single homozygous reporter mouse, while Experiment 2 included three homozygous reporter mice belonging to the same litter. A representative flow cytometry analysis of the Pcdh7-ZsGreen reporter mouse from experiment 1 shows the workflow for gating and selecting ZsGreen+ cells in the 6 different populations (Fig 3.4). In both Experiment 1 and 2, the ZsGreen+ cells only show a detectable shift from the ZsGreen- cells in the Lin-, LSKs, and ST-HSC populations. In the remaining cell types, the ZsGreen+ cells were identified with the help

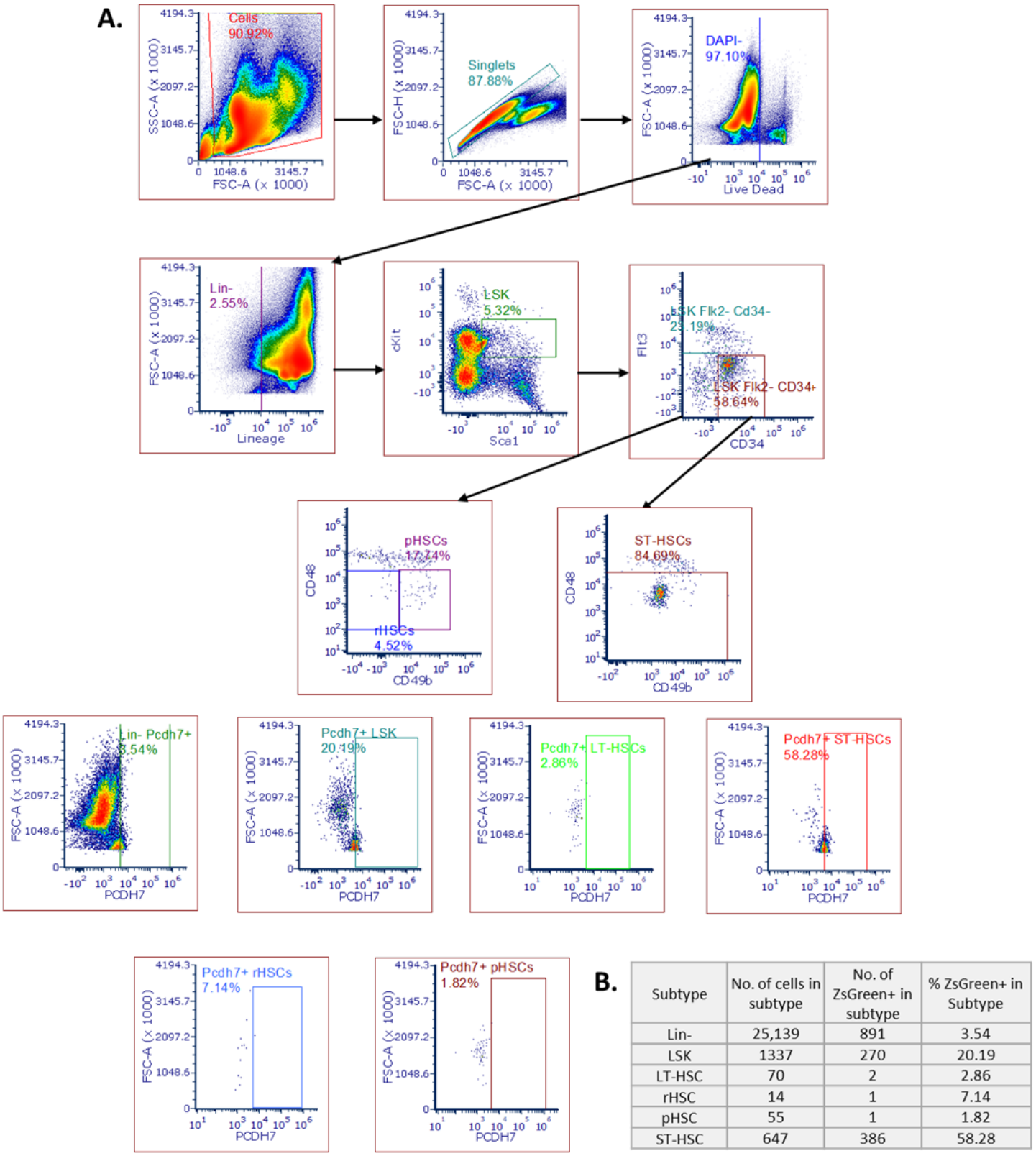

B.

Subtype	No. of cells in subtype	No. of ZsGreen+ in subtype	% ZsGreen+ in Subtype
Lin-	25,139	891	3.54
LSK	1337	270	20.19
LT-HSC	70	2	2.86
rHSC	14	1	7.14
pHSC	55	1	1.82
ST-HSC	647	386	58.28

Figure 3.4: A) Flow cytometry analysis workflow for selecting ZsGreen+ HSCs to check Pcdh7-ZsGreen expression in Experiment 1. 6 subpopulations were analysed: Lin-, LSKs, LT-HSCs, ST-HSCs, rHSCs and pHSCs. B) Table showing total number of cells within each subpopulation analyzed, number of ZsGreen+ cells within them and the percentage of ZsGreen+ cells in the subpopulation

of FMOs due to fewer cell numbers and the absence of a clear shift. The number of cells within each population in the Pcdh7-ZsG reporter mouse in experiment 1, the number of ZsGreen+ cells detected within each population and the percentage of Pcdh7-ZsGreen+ cells are given in Fig 3.4.B. ST-HSCs have the highest ZsGreen+ population (58.28%) followed by LSKs (20.19%). rHSCs and pHSCs have very few ZsGreen+ cells within them.

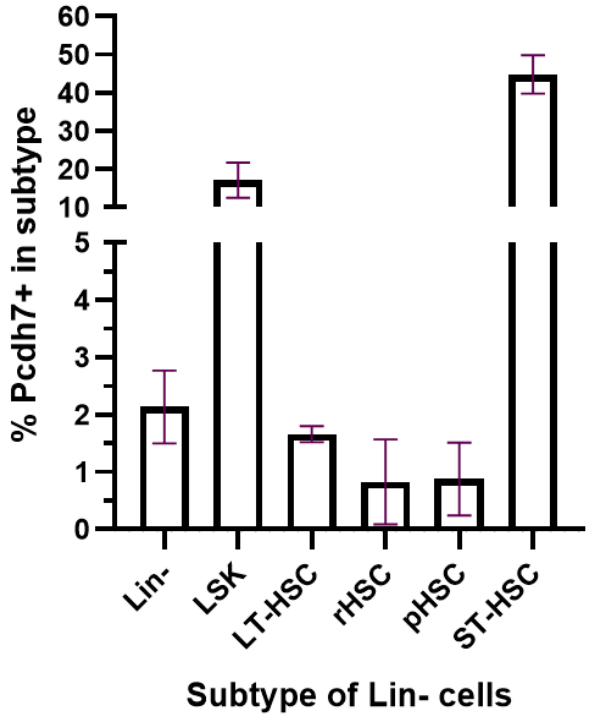

Figure 3.5: Percentage of ZsGreen detected by flow cytometry in the three Pcdh7-ZsG mice from Experiment 2. The error bars represent standard error from mean.

Figure 3.5 represents the percentage of ZsGreen+ cells detected within each subtype for Experiment 2. The error bars represent the standard error from the mean and show the variability within the replicates. ST-HSCs have the highest percentage of ZsGreen+ cells with a mean value of 44.7% followed by LSKs with a mean value of 17.1%. rHSCs and pHSCs have very few ZsGreen+ cells and have high variability. ST-HSCs may be the predominant ZsGreen+ population within LSKs.

A.

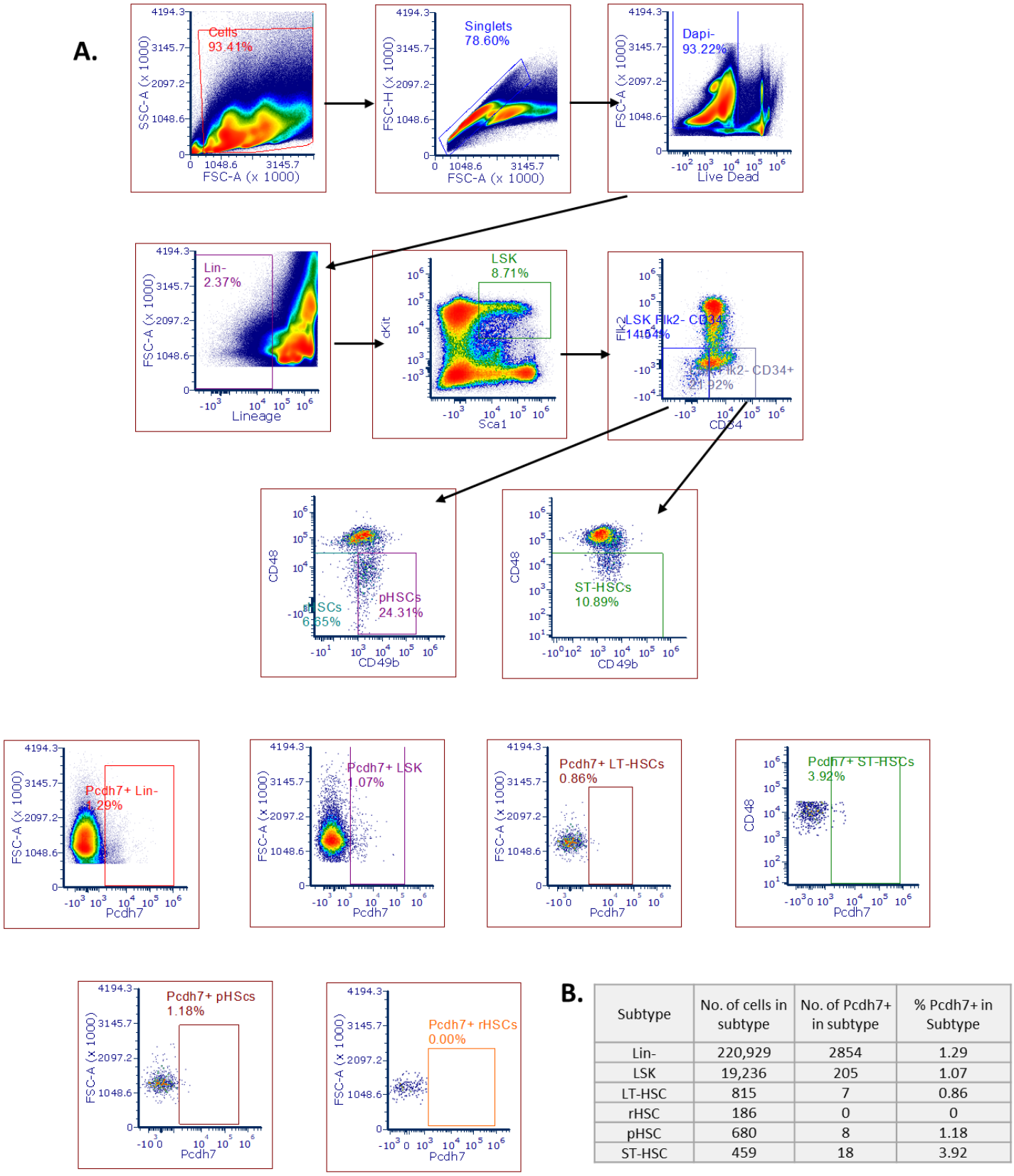

B.

Subtype	No. of cells in subtype	No. of Pcdh7+ in subtype	% Pcdh7+ in Subtype
Lin-	220,929	2854	1.29
LSK	19,236	205	1.07
LT-HSC	815	7	0.86
rHSC	186	0	0
pHSC	680	8	1.18
ST-HSC	459	18	3.92

Figure 3.6: A) Flow cytometry analysis workflow for selecting Pcdh7 + HSCs to check Pcdh7 expression in WT mice. 6 subpopulations were analyzed; Lin-, LSKs, LT-HSCs, ST-HSCs, rHSCs and pHSCs. B) Table showing total number of cells within each subpopulation analyzed, number of Pcdh7+ cells within them and the percentage of Pcdh7+ cells in the subpopulation

3.2.2 Flow cytometry analysis of WT mice using anti-Pcdh7 antibody

The bone marrow from WT mice was stained against Pcdh7 using an anti-Pcdh7 antibody. A representative flow cytometry analysis shows the workflow for gating and selecting Pcdh7+ cells in the 6 different populations (Fig 3.6.A). The Pcdh7+ cells were identified with the help of FMOs due to less cell number and the absence of a clear shift between the Pcdh7+ and Pcdh7- populations. The number of Pcdh7+ cells detected within each population and the percentage of Pcdh7-ZsGreen+ cells are given in Figure 3.6.B. ST-HSCs have the highest percentage of Pcdh7+ cells (3.9%)

3.2.3 Comparison between Pcdh7+ detection by ZsGreen expression and anti-Pcdh7 staining

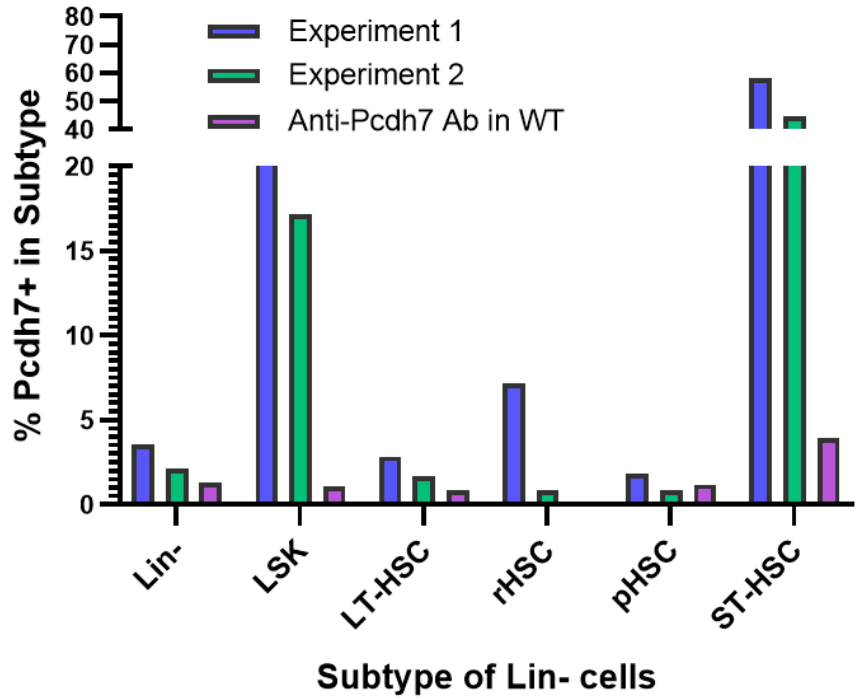

Figure 3.7: Comparison between Pcdh7+ cells detected by flow cytometry analysis in Pcdh7-ZsG mice. (by ZsGreen expression) and WT mice (by anti-Pcdh7 staining). Experiment 1 includes one homozygous Pcdh7-ZsG mouse and Experiment 2 includes three homozygous reporter mice replicates.

Figure 3.7 represents a comparison between the Pcdh7+ cell percentages detected by flow cytometry analysis across multiple flow cytometry experiments. The percentages shown for each cell type in Experiment 2 represent the mean value for the three replicates. ST-HSCs emerge as the predominant Pcdh7+ cell population for all three experiments. All the other cell types show highly variable percentages of Pcdh7+ cells. High variability is observed in the number of cells detected by antibody staining as compared to the endogenous ZsGreen tag. This suggests that further confirmatory experiments are needed to check Pcdh7 protein expression on HSCs. The findings suggest that ST-HSCs might be the predominant Pcdh7 expression population within HSCs as compared to rHSCs and pHSCs.

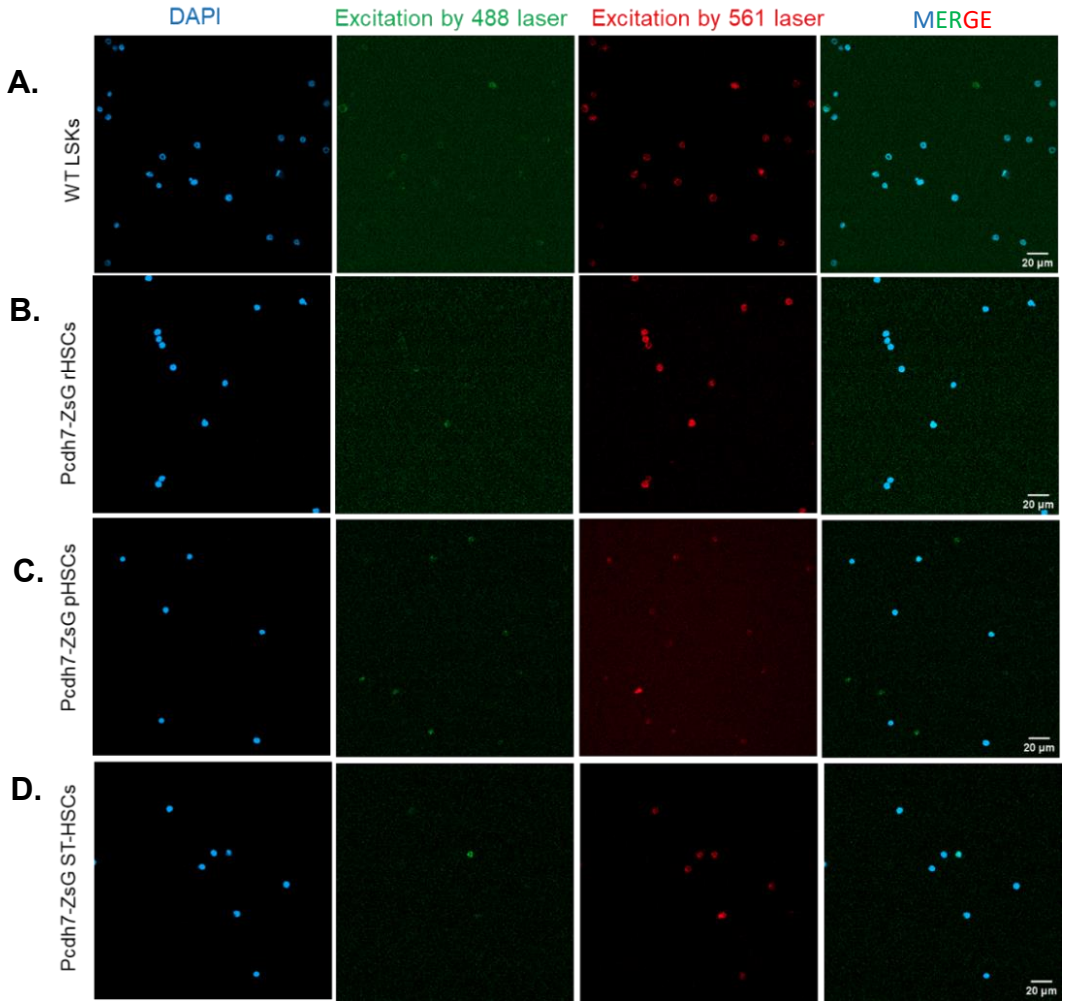

Figure 3.8: Representative images of flow cytometry sorted single cells after immunostaining at 40X magnification. Blue represents DAPI staining of the nucleus. Green represents excitation by the 488nm laser. Red represents excitation by 561nm laser. Alexa fluor 546 secondary antibody was used to tag the anti-ZsGreen primary antibody. A) WT LSK cells serve as the negative control for ZsGreen. B) rHSCs, C) pHSCs and D) ST-HSCs were sorted from Pcdh7-ZsG reporter mice

3.3 Flow cytometry sorting of HSC subtypes and single-cell immunostaining staining against ZsGreen produced inconclusive results

The flow cytometry analysis only gives a suggestive percentage of the Pcdh7+ cells within the rHSCs, pHSCs and ST-HSCs. To confirm the expression of Pcdh7 within specific HSC subtypes, the cells were sorted and stained after fixation. Due to the unavailability of a commercial anti-Pcdh7 antibody that specifically binds to Pcdh7, the anti-ZsGreen antibody validated in 3.1 was utilized for single cell staining.

rHSCs, pHSCs and ST-HSCs were sorted from Pcdh7-ZsG reporter mice and stained using the anti-ZsGreen antibody and DAPI. LSK cells from WT mice served as a negative control for ZsGreen expression. Figure 3.8 shows representative confocal microscopy images of the sorted cells at 40X magnification. On excitation by laser of 488 nm wavelength, weak green signals are observed in all the sorted cell populations (rHSCs, pHSCs and ST-HSCs) from the reporter mice which are also observed in WT LSKs.

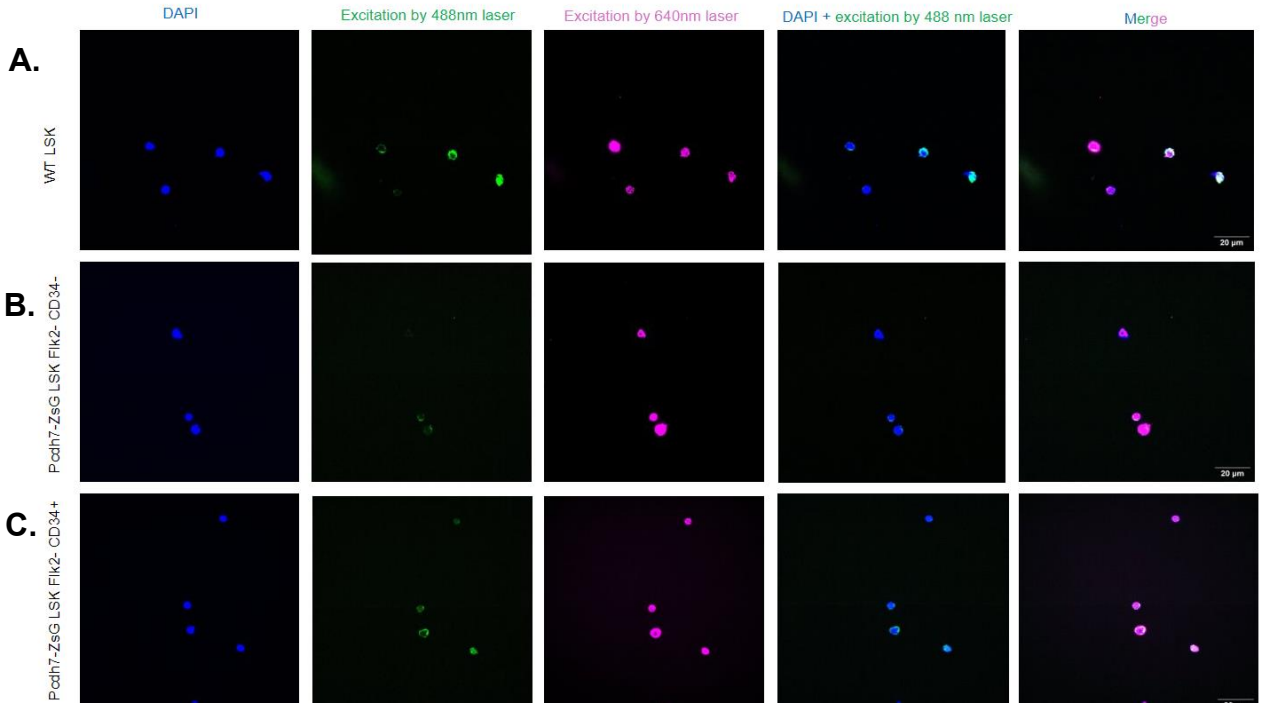

Figure 3.9: Representative images of flow cytometry sorted LSKs after immunostaining at 40X magnification. Blue represents DAPI staining of the nucleus. Green represents excitation by the 488nm laser. Magenta represents excitation by 640nm laser. Alexa fluor 647 secondary antibody was used to tag the anti-ZsGreen primary antibody. A) WT LSK cells serve as the negative control for ZsGreen. B) rHSCs, C) pHSCs and D) ST-HSCs were sorted from Pcdh7-ZsG reporter mice

Moreover, the anti-ZsGreen antibody does not show specificity towards ZsGreen and binds to both WT LSKs and HSCs from the Pcdh7-ZsG reporter mice.

The experiment was repeated to sort and immunostain Flk2- CD34- LSK cells which are the parent population for LT-HSCs and Flk2- CD34+ LSK cells which contain the ST-HSC population (Fig 3.9). WT-LSKs were sorted and stained as a negative control for ZsGreen expression. No ZsGreen+ cells were observed on excitation by the 488nm laser and cells

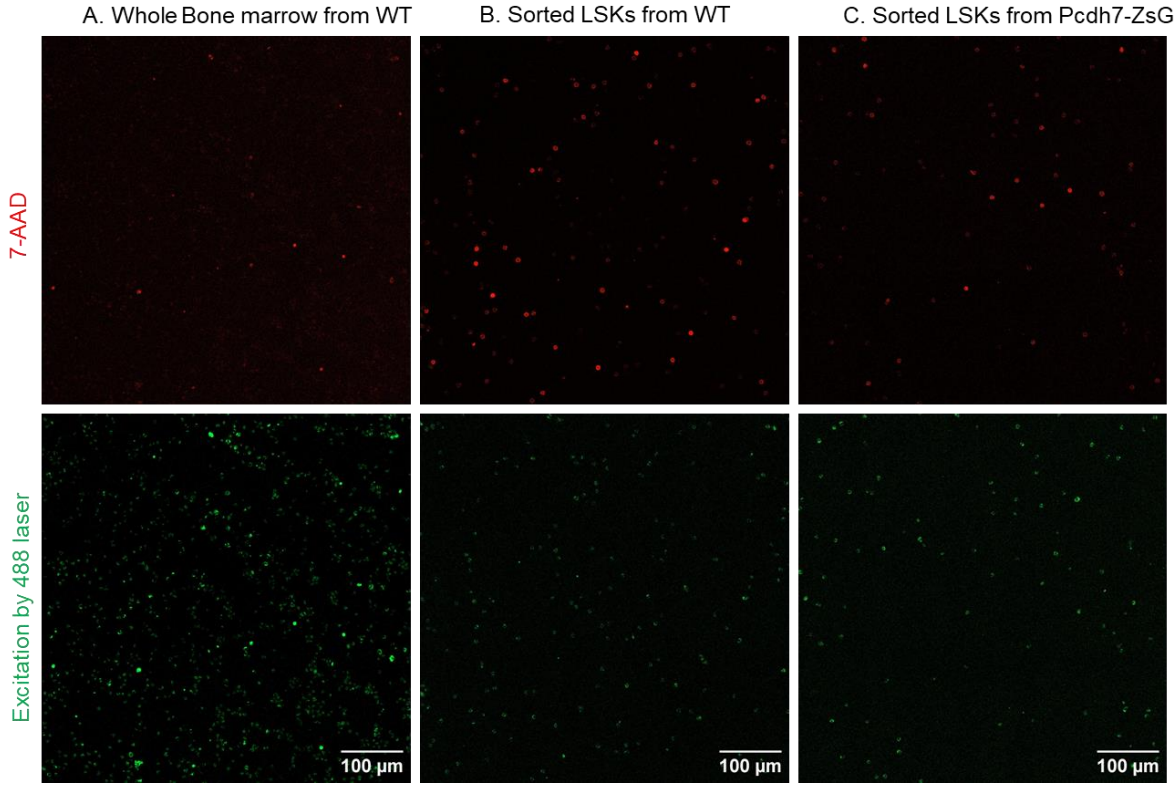

Figure 3.10: Representative images of flow cytometry sorted single cells without immunostaining at 40X magnification. The cells were sorted using 7AAD as nuclear represents excitation by the 488nm laser. Red represents excitation by 561 nm stain. Green laser. A) Whole bone marrow cells from WT mice without staining for flow cytometry sorting . B) LSKs sorted from WT mice, C) LSKs sorted from Pcdh7-ZsG mice

from both the WT control and Pcdh7-ZsG reporter mice showed weak green autofluorescence. The anti-ZsGreen antibody did not show specificity towards ZsGreen as it bound to all the cells. Further optimization of the single-cell immunostaining protocol is required to identify ZsGreen expressing HSCs.

To prevent potential interference from antibodies used for flow cytometry sorting imaging, bone marrow samples from both wild-type (WT) and Pcdh7-ZsG mice were stained for LSKs using fluorophores that do not get excited by the 488nm laser and were then sorted. Additionally, whole bone marrow cells from WT mice served as a control for autofluorescence. The cells were fixed after sorting to image for ZsGreen. 7AAD on the sorted cells served as an indicator for nuclear staining during imaging. Green signals were observed in both whole bone marrow and LSKs from WT mice, as well as LSKs from Pcdh7-ZsG reporter mice, which could be attributed to autofluorescence. A clear green signal indicative of ZsGreen expression was not detected in any of the LSK cells from Pcdh7-ZsG reporter mice (Fig 3.10)

3.4 Immunofluorescence staining of Pcdh7-ZsGreen femur sections show few potential ZsGreen+ cells.

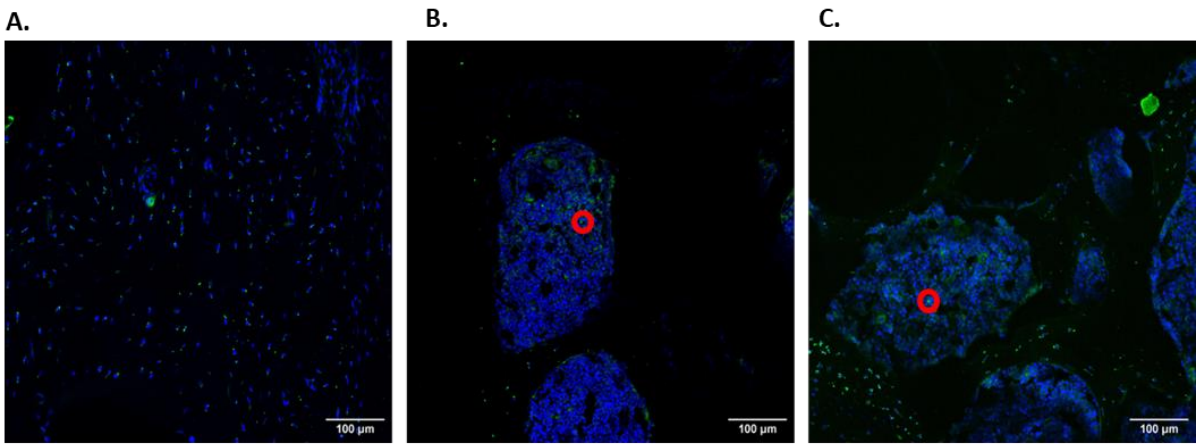

Figure 3.11: Representative images of DAPI stained tissue sections from Pcdh7-ZsG reporter mice at 40X magnification. Green represents the endogenous ZsGreen signal. A) Bone cells express Pcdh7-ZsGreen. B), C) Few bright green cells (circled) are detected within the bone marrow which are potential ZsGreen+ HSCs.

The flow cytometry analysis data from Pcdh7-ZsG reporter mice suggest that a small percentage of HSCs are Pcdh7-ZsGreen+. However, due to the highly heterogeneous nature of bone marrow, the probability of detecting them is low. To test if ZsGreen+ HSCs can be observed within the bone marrow and to study their localization within the trabecular bone area (TBA) and central marrow (CM) of the femur, immunofluorescence staining of tissue sections from Pcdh7-ZsG mouse femur was conducted.

Tissue sections of 10um thickness were obtained from Pcdh7-ZsG mouse femur fixed using 4% PFA. DAPI staining was used to visualize the bone marrow cells. Bright ZsGreen signals were observed in the regions where bone cells are present (Fig 3.11.A). On spectral unmixing of these signals, the emission spectrum peaks at 506nm and overlaps with the emission peak of ZsGreen from hippocampal sections (Fig 3.12.B). Hence, the bone cells serve as an internal comparison for ZsGreen within the mouse femur. Despite observing bright ZsGreen signals in bone regions, only a few ZsGreen+ cells were found within the bone marrow in multiple sections from Pcdh7-ZsG reporter mice (Fig. 3.11.B and 3.11.C) and were equally distributed between the TBA and CM. To confirm ZsGreen expression and their identity as HSCs, further staining is required using the anti-ZsGreen antibody and specific markers for HSCs. Excitation by the 488nm laser revealed green autofluorescence within all the cells of the bone marrow (Fig 3.13.A).

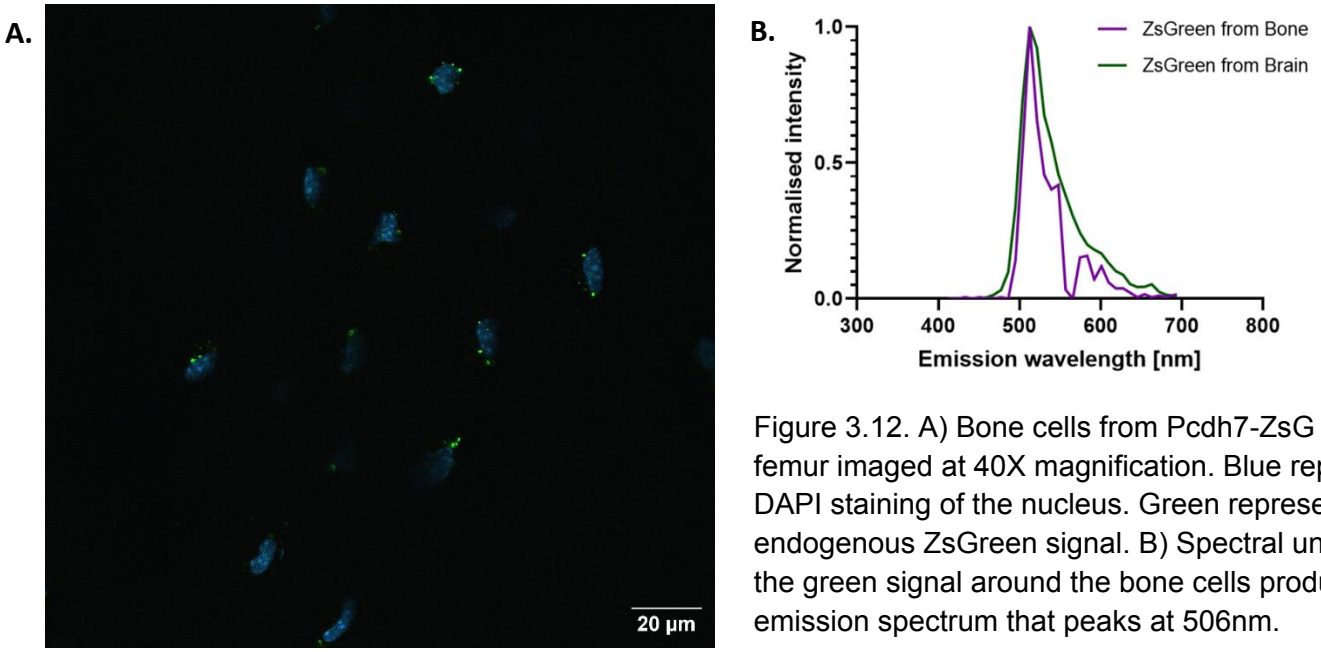

Figure 3.12. A) Bone cells from Pcdh7-ZsG mouse femur imaged at 40X magnification. Blue represents DAPI staining of the nucleus. Green represents endogenous ZsGreen signal. B) Spectral unmixing of the green signal around the bone cells produces an emission spectrum that peaks at 506nm.

Spectral unmixing of the potential ZsGreen signal from the bone marrow revealed a broader peak as compared to the peak from the ZsGreen in the bone, which could be due to a combination of weak ZsGreen signal and autofluorescence (Fig 3.13.C).

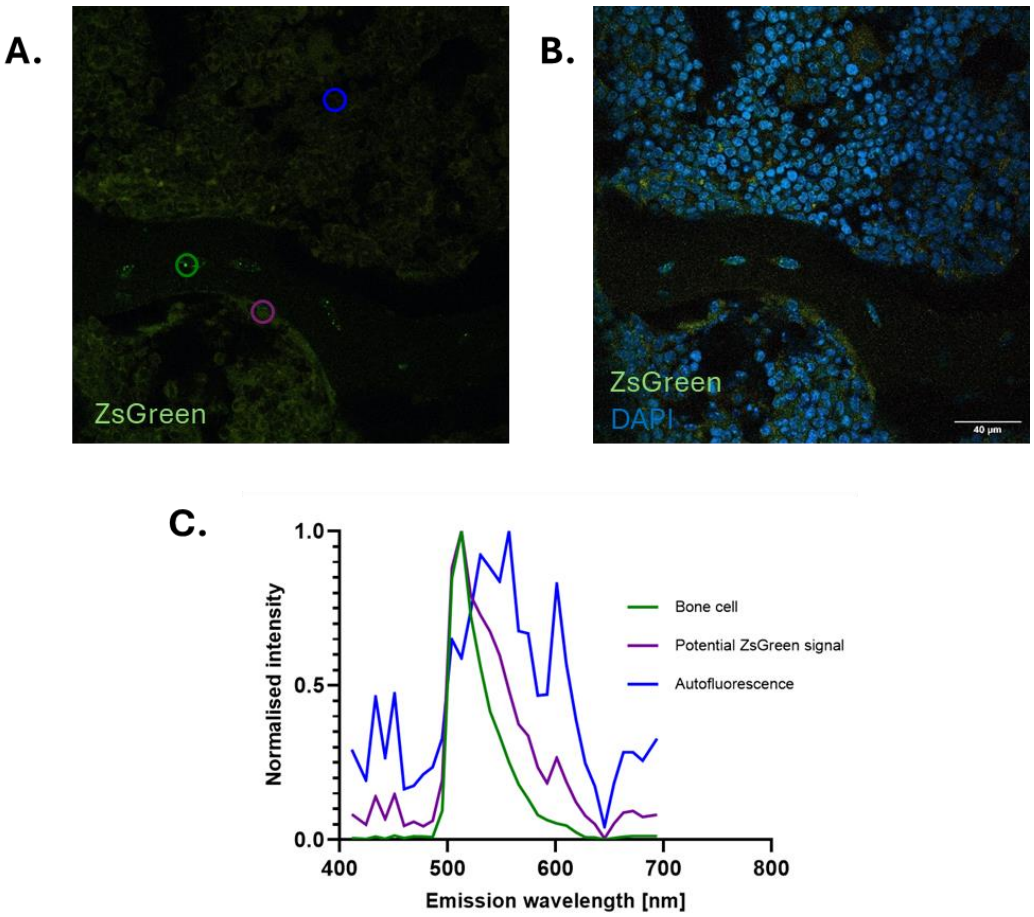

Figure 3.13. Representative confocal images of the bone marrow at 40X magnification. Green represents endogenous ZsGreen. Blue represents DAPI. A) Regions used for spectral unmixing are circled. B) DAPI reveals nuclear staining of cells. C) Spectral unmixing reveals a broader emission peak for potential ZsGreen signal within the bone marrow as compared to the narrow emission peak for ZsGreen signal from bone cells

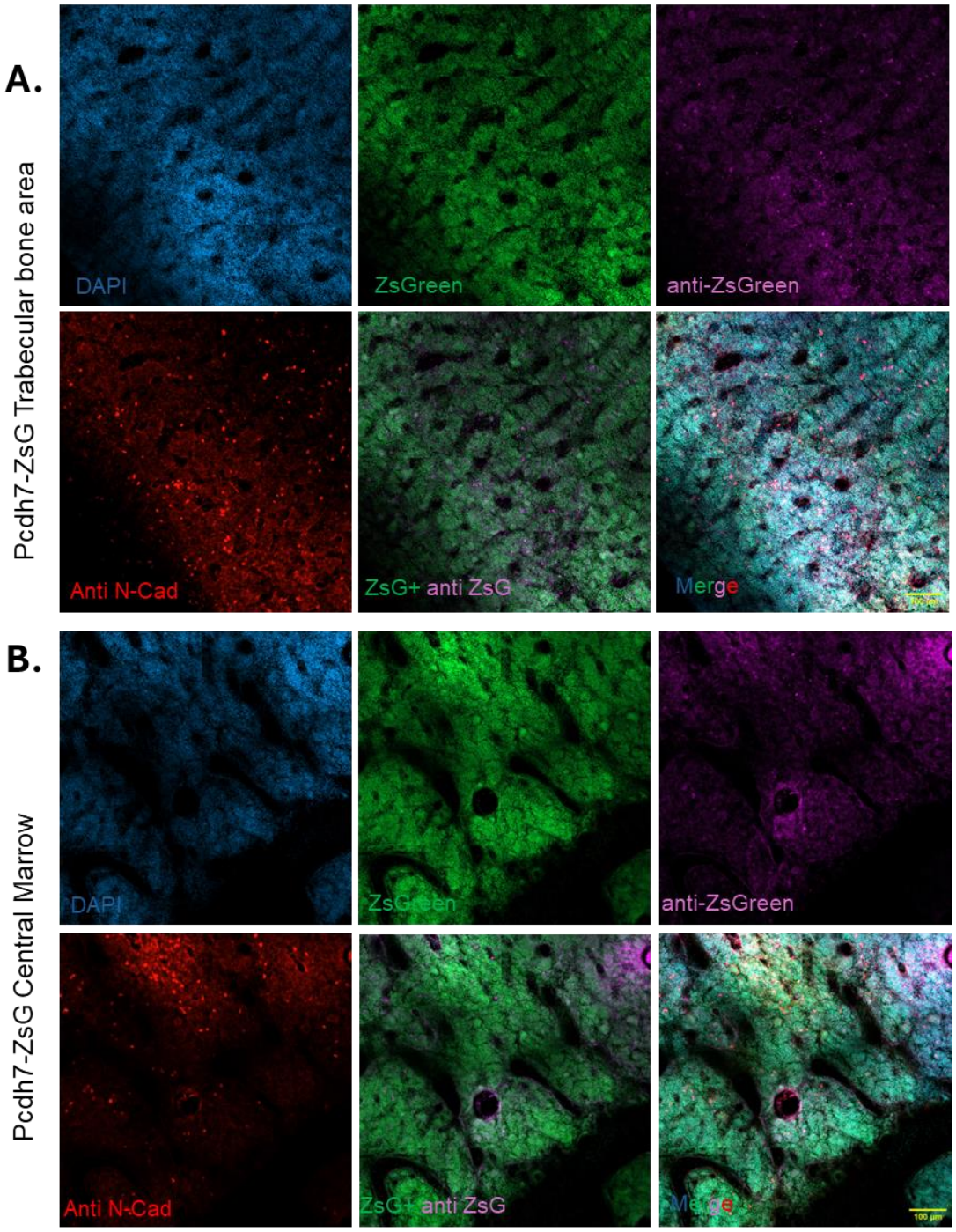

Figure 3.14. Z projection images showing whole mount immunostaining of Pcdh7-ZsG mouse femur at 40X magnification. Blue represents DAPI staining of nuclei. Green represents ZsGreen. Magenta represents anti-ZsGreen antibody. Red represents anti-N Cadherin staining. A) Images of the Trabecular bone area of the bone marrow B) Images of the Central Marrow region of the bone marrow. ZsGreen signals cannot be differentiated from the high autofluorescence of the bone marrow cells.

3.5 Whole-mount immunostaining of Pcdh7-ZsG femurs does not show ZsGreen in the bone marrow

Whole mount immunostaining was also used to observe the spatial localization of ZsGreen+ HSCs within the bone marrow and to understand the microenvironment that the cells are located within. For each fluorescent protein, the ideal tissue-clearing method varies and needs to be optimized. Due to time constraints, optimizations were not conducted, and a previously established protocol was used for the experiment.

As a pilot experiment, the bisected mouse femur was immunostained with DAPI, anti-ZsGreen and anti-N Cadherin, which is a marker for MSCs. Figure 3.14 shows Z-projections of whole mount images of the TBA and CM at 40X magnification. On excitation by the 488 nm laser, endogenous ZsGreen expressing cells could not be differentiated from the high autofluorescence. The Alexa Fluor 647 antibody used to tag anti-ZsGreen shows residual accumulation in the Z-slices within the first 50um of the bone marrow imaged, indicating that longer PBS washes are needed after secondary antibody staining to remove the unconjugated dye. The anti-N-Cadherin antibody effectively marked MSCs within the bone marrow.

3.6 Ex-vivo imaging of bone marrow preserves bone marrow architecture to image ZsGreen+ cells.

The EVISC technique can be used to study the behavior of the Pcdh7-ZsGreen+ HSCs within the HSC niche outside the host once their localization within the bone marrow is identified and the subtype of HSC is identified. The imaging depth achievable with a two-photon confocal microscope is limited to 200 μm. Hence, the number of ZsGreen+ HSCs has to be sufficient to identify them within the complex bone marrow.

To validate the experimental setup, the conditions utilized by Xie et al. 2009 were replicated to check if further optimizations are necessary for this project. Bone fragments

from the TBA and CM of 2-3 mm height were cultured in DMEM medium to check whether the bone architecture is maintained without loss of bone marrow cells. The bone marrow from the Pcdh7-ZsG mouse was imaged using two-photon confocal microscopy to check if ZsGreen signals are visible within the bone marrow (Fig 3.15.A and B). The secondary harmonic signal from collagen was used to identify the bone. Spectral unmixing of the green signal emitted by the 488nm laser revealed a broad emission spectrum (Fig 3.15.C). Single cells expressing ZsGreen could not be identified within the bone marrow due to high autofluorescence.

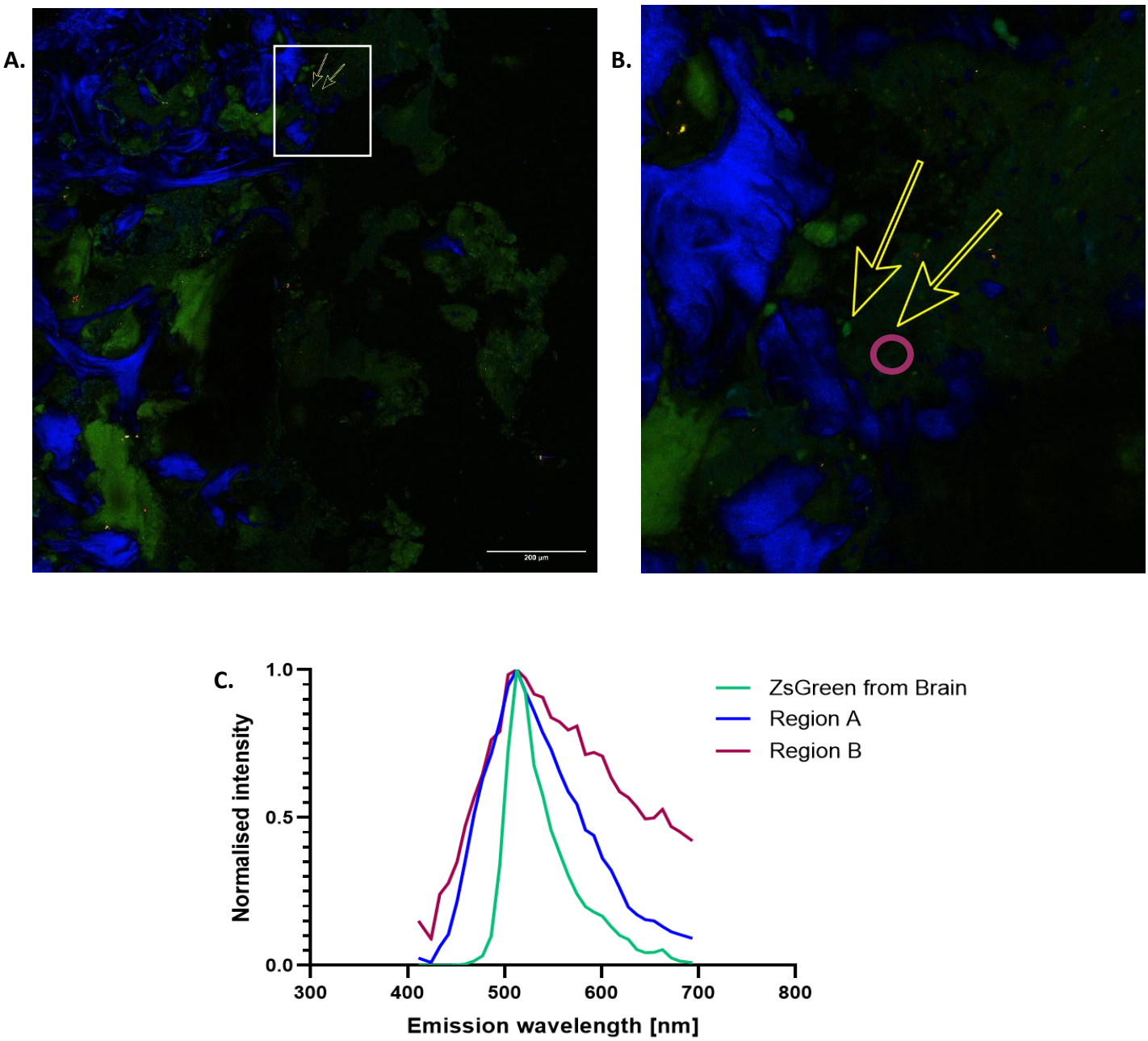

Figure 3.15. Representative two-photon microscopy images of the bone marrow at 40X magnification. Green represents endogenous ZsGreen. Blue represents DAPI. A) Tiled image of TBA region B) Zoom-in of marked area in image A. Regions used for spectral unmixing are circled. C) Spectral unmixing of marked regions in image B reveals a broader emission peak for regions A and B within the bone marrow as compared to the narrow emission peak for ZsGreen signal from brain

CHAPTER 4- Discussion

Bulk RNA sequencing data reveals higher expression of Pcdh7 RNA in primed HSCs as compared to reserve HSCs. As Pcdh7 is an adhesion protein, we hypothesized that it plays a role in LT-HSCs adopting the fate of pHSCs by modifying the adhesive interaction that the HSCs have with the niche, facilitating migration. From preliminary flow cytometry data, we see that Pcdh7 is not highly expressed in rHSCs or pHSCs and is not differentially expressed between them, only a fraction of these cells expresses Pcdh7. However, it is observed that ST-HSCs show a high percentage of Pcdh7 expression. There is no agreement between the Pcdh7 detected in cells by indirect measurement of ZsGreen+ cells and by using anti-Pcdh7 antibody. In a further study, different HSC populations like rHSCs, pHSCs, Flk2- CD34- cells and Flk2- CD34+ cells were sorted from Pcdh7-ZsG reporter mice and were fixed and stained for anti-ZsGreen. ZsGreen could not be detected in these cells and the antibody staining showed non-specific binding. On imaging sorted LSKs without anti-ZsGreen antibody staining from Pcdh7-ZsG mice, true ZsGreen signal could not be observed in any of the cells. Whole mount immunostaining of Pcdh7-ZsGreen femurs failed to detect ZsGreen+ cells within the bone marrow due to high autofluorescence. Very few ZsGreen+ cells were observed in tissue sections from Pcdh7-ZsG reporter mouse femurs and to confirm their identity as HSCs, further staining with HSC markers needs to be done.

4.1 Validation of Pcdh7 expression at the protein level

The current hypothesis is based on bulk-RNA sequencing data, which indicates Pcdh7 RNA expression within HSCs and does not directly correlate to Pcdh7 protein expression within HSCs. The differential expression of Pcdh7 RNA between rHSCs and pHSCs may not translate to a functional role for the protein. The data from the bulk RNA sequencing needs to be verified using techniques like RT-qPCR to further check its reliability.

Western blotting, which is a common technique for verification of protein expression and quantification cannot be used for this study as a large number of LT-HSCs will be required

for this. To validate protein expression within different subpopulations of HSCs, the current approach taken is flow cytometry analysis, which presents challenges as HSCs themselves are low in number. Pcdh7 expressing cells may be a very small fraction within HSCs which can go undetected. The lack of a clear separation between Pcdh7+ and Pcdh7- population makes it difficult to pinpoint the actual Pcdh7 expressing population.

As Pcdh7 is tagged to ZsGreen in Pcdh7-ZsG reporter mice, ZsGreen was used as an indirect measure of Pcdh7 expression. There is a discordance seen between the Pcdh7+ HSC number seen by analyzing ZsGreen signal in the reporter mice and by using an anti-Pcdh7 antibody in WT mice. When HSCs were sorted from the reporter mice, all cells showed green autofluorescence and true ZsGreen could not be observed within them. The anti-ZsGreen antibody validated on hippocampal tissue sections shows non-specific binding to all the sorted cells in both WT control LSKs and HSCs from Pcdh7-ZsG mice. The antibody staining and permeabilization method used need to be further optimized for this experiment.

Taking into consideration the interference of flow cytometry antibodies tagged to the cells, LSK cells were sorted from Pcdh7-ZsG mice without adding fluorophores that get excited by 488 nm laser during imaging. DAPI was also replaced by 7AAD as the excitation peak of DAPI lies close to that of ZsGreen. True ZsGreen signal could not be detected in any of the LSK cells from the reporter mice which may indicate that ZsGreen may be lost during processing of cells or very negligible number of cells express Pcdh7.

4.2 Whole mount immunostaining does not reveal conclusive data about the localization of Pcdh7-ZsGreen+ HSCs

Whole mount immunostaining of mouse femur from Pcdh7-ZsG mice failed to provide evidence regarding the localization of Pcdh7+ HSCs within the bone marrow. Strong autofluorescence in the bone marrow cells prevented the identification of true ZsGreen+ HSCs within the bone marrow. The number of HSCs might be insufficient to visualize using this method as only 200µm of the bone marrow can be imaged. There is also a

possibility of a loss of endogenous ZsGreen signal due to strong tissue clearing by BABB reagent. The whole-mount immunostaining protocol needs to be optimized for ZsGreen with the usage of milder tissue-clearing reagents like glycerol, OPTIPREP, EasyIndex and Fruit.

As Pcdh7 is an adhesion protein, there is the possibility that Pcdh7+ cells of non-hematopoietic origin exist with the bone marrow that contribute to autofluorescence. Within this heterogeneity, Pcdh7+ HSCs can be identified by immunofluorescence staining against various HSC markers.

4.3 Not rHSCs or pHSCs, but ST-HSCs might be the predominant Pcdh7-expressing population.

rHSCs and pHSCs have very limited Pcdh7+ cells within them. Contrary to our initial hypothesis, flow cytometry analysis indicates the predominant expression of Pcdh7 to be within short-term HSCs (ST-HSCs). The bulk-RNA sequencing data shows some RNA expression in ST-HSCs, although lesser than pHSCs. Further studies need to be done to check if Pcdh7 is expressed in ST-HSCs. The flow analysis should be repeated multiple times to see if ST-HSCs still emerge as the higher Pcdh7-expressing population. This can also be validated using a Pcdh7-specific flow cytometry antibody. ST-HSCs can be sorted from reporter mice and analyzed to check ZsGreen expression.

4.4 Functional test to study Pcdh7+ HSCs

An alternative strategy to explore the functional significance of Pcdh7 expression in HSCs involves isolating Pcdh7-ZsGreen+ cells from Pcdh7-ZsGreen reporter mice to transplant them into irradiated recipient mice. This allows the assessment of their self-renewal capacity and multilineage differentiation potential. Post-transplantation, the peripheral blood can be analyzed to check the effect of Pcdh7+ HSCs on the blood cell pool as compared to the control mice. This can help understand the role of Pcdh7 in hematopoiesis.

References

Akashi, K, Traver, D, Miyamoto, T, and Weissman, IL (2000). A clonogenic common myeloid progenitor that gives rise to all myeloid lineages. Nature 404, 193–197.

Birbrair, A, and Frenette, PS (2016). Niche heterogeneity in the bone marrow. Ann N Y Acad Sci 1370, 82–96.

Bisogni, AJ, Ghazanfar, S, Williams, EO, Marsh, HM, Yang, JY, and Lin, DM (2018). Tuning of delta-protocadherin adhesion through combinatorial diversity. Elife 7, e41050.

Bruns, I, Lucas, D, Pinho, S, Ahmed, J, Lambert, MP, Kunisaki, Y, Scheiermann, C, Schiff, L, Poncz, M, Bergman, A, *et al.* (2014). Megakaryocytes regulate hematopoietic stem cell quiescence through CXCL4 secretion. Nat Med 20, 1315–1320.

Calvi, LM, Adams, GB, Weibrecht, KW, Weber, JM, Olson, DP, Knight, MC, Martin, RP, Schipani, E, Divieti, P, Bringhurst, FR, *et al.* (2003). Osteoblastic cells regulate the haematopoietic stem cell niche. Nature 425, 841–846.

Chen, H-F, Ma, R-R, He, J-Y, Zhang, H, Liu, X-L, Guo, X-Y, and Gao, P (2017). Protocadherin 7 inhibits cell migration and invasion through E-cadherin in gastric cancer. Tumour Biol 39, 1010428317697551.

Ding, L, Saunders, TL, Enikolopov, G, and Morrison, SJ (2012). Endothelial and perivascular cells maintain haematopoietic stem cells. Nature 481, 457–462.

Ellis, SL, Grassinger, J, Jones, A, Borg, J, Camenisch, T, Haylock, D, Bertoncello, I, and Nilsson, SK (2011). The relationship between bone, hemopoietic stem cells, and vasculature. Blood 118, 1516–1524.

Gao, X, Xu, C, Asada, N, and Frenette, PS (2018). The hematopoietic stem cell niche: from embryo to adult. Development 145, dev139691.

Hirabayashi, T, and Yagi, T (2014). Protocadherins in neurological diseases. Adv Neurobiol 8, 293–314.

Hirano, S, and Takeichi, M (2012). Cadherins in Brain Morphogenesis and Wiring | Physiological Reviews. Physiological Reviews, 597–634.

Hulpiau, P, and van Roy, F (2009). Molecular evolution of the cadherin superfamily. The International Journal of Biochemistry & Cell Biology 41, 349–369.

Kiel, MJ, Yilmaz, ÖH, Iwashita, T, Yilmaz, OH, Terhorst, C, and Morrison, SJ (2005). SLAM Family Receptors Distinguish Hematopoietic Stem and Progenitor Cells and Reveal Endothelial Niches for Stem Cells. Cell 121, 1109–1121.

Köhler, A, Schmithorst, V, Filippi, M-D, Ryan, MA, Daria, D, Gunzer, M, and Geiger, H (2009). Altered cellular dynamics and endosteal location of aged early hematopoietic progenitor cells revealed by time-lapse intravital imaging in long bones. Blood 114, 290–298.

Kondo, M, Weissman, IL, and Akashi, K (1997). Identification of Clonogenic Common Lymphoid Progenitors in Mouse Bone Marrow. Cell 91, 661–672.

Laurenti, E, and Göttgens, B (2018). From haematopoietic stem cells to complex differentiation landscapes. Nature 553, 418–426.

Li, L, and Xie, T (2005). STEM CELL NICHE: Structure and Function. Annual Review of Cell and Developmental Biology 21, 605–631.

Lucas, D (2021). Structural organization of the bone marrow and its role in hematopoiesis. Curr Opin Hematol 28, 36–42.

Medvinsky, A, Rybtsov, S, and Taoudi, S (2011). Embryonic origin of the adult hematopoietic system: advances and questions. Development 138, 1017–1031.

Méndez-Ferrer, S, Michurina, TV, Ferraro, F, Mazloom, AR, MacArthur, BD, Lira, SA, Scadden, DT, Ma'ayan, A, Enikolopov, GN, and Frenette, PS (2010). Mesenchymal and haematopoietic stem cells form a unique bone marrow niche. Nature 466, 829–834.

Morrison, SJ, Hemmati, HD, Wandycz, AM, and Weissman, IL (1995). The purification and characterization of fetal liver hematopoietic stem cells. Proc Natl Acad Sci U S A 92, 10302–10306.

Morrison, SJ, Wandycz, AM, Hemmati, HD, Wright, DE, and Weissman, IL (1997). Identification of a lineage of multipotent hematopoietic progenitors. Development 124, 1929–1939.

Orkin, SH, and Zon, LI (2008). Hematopoiesis: An Evolving Paradigm for Stem Cell Biology. Cell 132, 631–644.

Pancho, A, Aerts, T, Mitsogiannis, MD, and Seuntjens, E (2020). Protocadherins at the Crossroad of Signaling Pathways. Frontiers in Molecular Neuroscience 13.

Pinho, S, and Frenette, PS (2019). Haematopoietic stem cell activity and interactions with the niche. Nat Rev Mol Cell Biol 20, 303–320.

Piper, M, Dwivedy, A, Leung, L, Bradley, RS, and Holt, CE (2008). NF-Protocadherin and TAF1 Regulate Retinal Axon Initiation and Elongation *In Vivo*. J Neurosci 28, 100–105.

Rashid, D, Puettmann, P, Roy, E, and Bradley, RS (2018). Neural crest development in Xenopus requires Protocadherin 7 at the lateral neural crest border. Mech Dev 149, 41–52.

Redies, C, Vanhalst, K, and Roy, F van (2005). delta-Protocadherins: unique structures and functions. Cell Mol Life Sci 62, 2840–2852.

Reya, T (2003). Regulation of hematopoietic stem cell self-renewal. Recent Prog Horm Res 58, 283–295.

Sano, K, Tanihara, H, Heimark, RL, Obata, S, Davidson, M, St John, T, Taketani, S, and Suzuki, S (1993). Protocadherins: a large family of cadherin-related molecules in central nervous system. The EMBO Journal 12, 2249–2256.

Schofield, R (1978). The relationship between the spleen colony-forming cell and the haemopoietic stem cell. A hypothesis. Blood Cells 4, 7–25.

Sugiyama, T, Kohara, H, Noda, M, and Nagasawa, T (2006). Maintenance of the hematopoietic stem cell pool by CXCL12-CXCR4 chemokine signaling in bone marrow stromal cell niches. Immunity 25, 977–988.

Takeichi, M (1988). The cadherins: cell-cell adhesion molecules controlling animal morphogenesis. Development 102, 639–655.

Till, JE, and McCulloch, EA (1961). A Direct Measurement of the Radiation Sensitivity of Normal Mouse Bone Marrow Cells. Radiation Research 14, 213–222.

Vanhalst, K, Kools, P, Staes, K, van Roy, F, and Redies, C (2005). delta-Protocadherins: a gene family expressed differentially in the mouse brain. Cell Mol Life Sci 62, 1247–1259.

Wang, C, Chen, A, Ruan, B, Niu, Z, Su, Y, Qin, H, Zheng, Y, Zhang, B, Gao, L, Chen, Z, *et al.* (2020a). PCDH7 Inhibits the Formation of Homotypic Cell-in-Cell Structure. Front Cell Dev Biol 8.

Wang, Y, Kerrisk Campbell, M, Tom, I, Foreman, O, Hanson, JE, and Sheng, M (2020b). PCDH7 interacts with GluN1 and regulates dendritic spine morphology and synaptic function. Sci Rep 10, 10951.

Wu, Q, and Maniatis, T (1999). A Striking Organization of a Large Family of Human Neural Cadherin-like Cell Adhesion Genes. Cell 97, 779–790.

Xie, Y, Yin, T, Wiegraebe, W, He, XC, Miller, D, Stark, D, Perko, K, Alexander, R, Schwartz, J, Grindley, JC, *et al.* (2009). Detection of functional haematopoietic stem cell niche using real-time imaging. Nature 457, 97–101.

Yagi, T (2012). Molecular codes for neuronal individuality and cell assembly in the brain. Frontiers in Molecular Neuroscience 5.

Yamazaki, S, Ema, H, Karlsson, G, Yamaguchi, T, Miyoshi, H, Shioda, S, Taketo, MM, Karlsson, S, Iwama, A, and Nakauchi, H (2011). Nonmyelinating Schwann cells maintain hematopoietic stem cell hibernation in the bone marrow niche. Cell 147, 1146–1158.

Yang, L, Bryder, D, Adolfsson, J, Nygren, J, Månsson, R, Sigvardsson, M, and Jacobsen, SEW (2005). Identification of Lin(-)Sca1(+)kit(+)CD34(+)Flt3- short-term hematopoietic stem cells capable of rapidly reconstituting and rescuing myeloablated transplant recipients. Blood 105, 2717–2723.

Yang, Z, Dong, R, Mao, X, He, XC, and Li, L (2024). Stress-protecting harbors for hematopoietic stem cells. Curr Opin Cell Biol 86, 102284.

Yin, T, and Li, L (2006). The stem cell niches in bone. J Clin Invest 116, 1195–1201.

Yoshida, K, Yoshitomo-Nakagawa, K, Seki, N, Sasaki, M, and Sugano, S (1998). Cloning, expression analysis, and chromosomal localization of BH-protocadherin (PCDH7), a novel member of the cadherin superfamily. Genomics 49, 458–461.

Zhang, J, Niu, C, Ye, L, Huang, H, He, X, Tong, W-G, Ross, J, Haug, J, Johnson, T, Feng, JQ, *et al.* (2003). Identification of the haematopoietic stem cell niche and control of the niche size. Nature 425, 836–841.

Zhao, M, Tao, F, Venkatraman, A, Li, Z, Smith, SE, Unruh, J, Chen, S, Ward, C, Qian, P, Perry, JM, *et al.* (2019). N-Cadherin-Expressing Bone and Marrow Stromal Progenitor Cells Maintain Reserve Hematopoietic Stem Cells. Cell Rep 26, 652-669.e6.

Zhao, M, Perry, JM, Marshall, H, Venkatraman, A, Qian, P, He, XC, Ahamed, J, and Li, L (2014). Megakaryocytes maintain homeostatic quiescence and promote post-injury regeneration of hematopoietic stem cells. Nat Med 20, 1321–1326